A single-mode associates global patterns of brain network structure and behavior across the human lifespan

Brent McPherson[1] and Franco Pestilli[1,2]

Author Information

1. Department of Psychological and Brain Sciences, Indiana University Bloomington, 1101 E 10th Street, Bloomington, Indiana USA 47405. EMAIL: bcmcpher@iu.edu.
2. Department of Psychological and Brain Sciences, Indiana University, 1101 E 10th Street, Bloomington, Indiana USA 47405.
3. Department of Psychology, The University of Texas at Austin, 108 E. Dean Keeton St., Austin, TX 78712 https://orcid.org/0000-0002-2469-0494 URL: https://liberalarts.utexas.edu/psychology/faculty/fp4834, EMAIL: pestilli@utexas.edu

Corresponding authors Franco Pestilli pestilli@utexas.edu

Abstract

Multiple human behaviors improve early in life, peaking in young adulthood, and declining thereafter. Several properties of brain structure and function progress similarly across the lifespan. Cognitive and neuroscience research has approached aging primarily using associations between a few behaviors, brain functions, and structures. Because of this, the multivariate, global factors relating brain and behavior across the lifespan are not understood. We investigated the global patterns of associations between 334 behavioral and clinical measures and 376 brain structural connections in 594 individuals across the lifespan. A single-axis associated changes in multiple behavioral domains and brain structural connections (r=0.5808). Individual variability within the single association-axis well predicted the subjects age (r=0.6275). Representational similarity analysis evidenced global patterns of interactions across multiple brain networks systems and behavioral domains. Results show that a global process of human aging is well captured by multivariate data fusion approach. [147]

Data availability

The source data are provided by the Cambridge Aging Neuroscience Project https://camcan-archive.mrc-cbu.cam.ac.uk/. Brain data derived as part of this project and used as features for all the analyses are available on brainlife.io/pubs: <DOI>

Code availability

Code is available on github at https://github.com/bcmcpher/cca_aging and as web services reproducing the analyes at <URL>

Acknowledgments

This research was supported by NSF OAC-1916518, NSF IIS-1912270, NSF IIS-1636893, NSF BCS-1734853, Microsoft Faculty Fellowship to F.P., NIH 5T32MH103213-05 to William Hetrick. We thank Soichi Hayashi, Brad Caron and Josh Faskowitz for contributing to the development of brainlife.io, Craig Stewart, Robert Henschel, David Hancock and Jeremy Fischer for support with jetstream-cloud.org (NSF ACI-1445604).

Introduction

Understanding human aging and its progression in health and disease has become a critical need due to the rapidly aging world population (Nations and United Nations; Rich and Barry). Brain aging and the associated cognitive decline negatively impacts society by reducing the independence of individuals in the population, with significant costs associated with increased needs for long term support or treatment (Lustig et al.; Deary et al.; Niccoli and Partridge; Risacher and Saykin; Harada et al.). Costs associated with an aging population are only expected to increase over the next years, given the increase in life expectancy (Wykes et al.; DiLuca and Olesen; Gustavsson et al.; Andlin-Sobocki et al.; Wittchen et al.). As a result of this looming demographic shift, improving prodromal identification of individuals at risk versus individuals subject to normal aging in large human populations is becoming a priority (Taylor et al.; Vinke et al.; Beaton et al.; Veitch et al.; Svaldi et al.).

The normative human aging process is accompanied by behavioral changes in performance in both cognitive and perceptual tasks across the lifespan (Park and Reuter-Lorenz; Cepeda et al.; Amunts et al.). Early work focussed on measuring cognitive and perceptual aging with deep characterization of a few behavioral tasks (Salthouse, *Theoretical Perspectives on Cognitive Aging*; Salthouse, "Trajectories of Normal Cognitive Aging"; Cabeza et al.; Kramer et al.). A staggering amount of evidence has been reported on the effect of aging to human cognition and perception. For example, language processing and letter perception deteriorate with age (Salthouse, "What and When of Cognitive Aging"; Ratcliff, Thapar, Gomez, et al.; Thapar et al.). At the same time, visual contrast sensitivity, motion detection, recognition and iconic memory also decay across the lifespan (Lisman et al.; Nyberg and Pudas; Lu et al.; Sekuler and Hutman; Bennett et al.). Yet, this is not always the case as resilience to the effect of aging has been reported in a few behavioral domains such as language (Ratcliff, Thapar, Gomez, et al.; Ratcliff, Thapar, and McKoon; Thapar et al.) (e.g., vocabulary size) and emotion (Samanez-Larkin et al.; Carstensen et al.).

Correspondingly with cognitive aging, brain aging is associated with both changes to neuronal structures and function (Mok et al.; Gaetz et al.; Tsvetanov et al.; Grady; Salthouse, *Theoretical Perspectives on Cognitive Aging*; Grady et al.; Fjell et al.; Johnson et al.). Primary examples of changes to brain structures consist of hippocampal volume reduction (Apostolova et al.; Driscoll et al.), cortical thinning (Habes et al.; Salat et al.), and ventricular expansion (Fjell et al.). At the same time, multiple examples of changes in the brain functional activity have been reported (Maillet and Rajah; Paxton et al.). For example, the brain hemodynamic response changes across age (Huettel et al.; D'Esposito et al.; Buckner et al.), prefrontal cortex activity changes during a variety of tasks (H.-J. Li et al.; Maillet and Rajah; Reuter-Lorenz and Lustig), such as attentional control (Milham et al.; Gordon et al.), inhibition (Milham et al.; Gazzaley et al.), and executive control (Cepeda et al.). Finally, changes to the white matter tissue properties across the lifespan have been reported (Yeatman et al.; Thomason and Thompson; Reisberg et al.; Cox et al.; Xu et al.; Zuo et al.; Salthouse, "Neuroanatomical Substrates of Age-Related Cognitive Decline"; Wandell). These studies painted a comprehensive picture of how aging affects human behavior due to alterations to either brain function and structure across multiple tissue types.

As of today, much attention has been devoted to characterization of the changes in individual cognitive tasks and brain systems as a result of aging (Salthouse, *Theoretical Perspectives on Cognitive Aging*; Buckner et al.; Gutchess). This approach has helped tremendously in developing an understanding of the mechanisms involved in individual cognitive functions (Oschwald et al.; Cole and Franke; Cole et al.; Bishop et al.). Yet, a few shortcomings have been noted with single-task approaches (Turner et al.; Falk et al.). For example, limits to the definition of psychological constructs (Poldrack; Mok et al.), and the co-involvement of networks of brain systems in supporting individual psychological domains (Zuo et al.; Bassett and Sporns; van den Heuvel and Sporns; Petersen and Sporns) hinder our ability to assign a one-to-one correspondence between brain systems and psychological constructs or tasks. For example, challenges in isolating cognitive processes (Braun et al.; Khambhati et al.; Rutter et al.; Maunsell), resulted in critiques to the very definition of psychological constructs (Poldrack). Furthermore, studying a few constructs at a time may be also limited because multiple processes coexist within individual brain areas, as early as in the sensory systems (Semedo et al.; Huk).

Besides the mappings between a few functions and brain systems, the global patterns of change in the brain network connectivity associated with human aging, behavior and cognition remain uncharted. To advance understanding of normative aging, we integrated multivariate (Tsvetanov et al.; Grady et al.; Braun et al.; McIntosh and Mišić; S. M. Smith et al.; Llera et al.) and network neuroscience (Kong et al.; Morgan et al.; Davis et al.; Tsvetanov et al.; Daianu et al.) methods to develop a "many-to-many" map between behavioral domains and brain network systems. A reproducible data preprocessing pipeline was developed for the current work and made freely available as a web service on brainlife.io (Avesani et al.). The pipeline was used to process data from a large sample of healthy adults (594 subjects, 18-88 years; (Shafto et al.)). Canonical Correlation Analysis (CCA; (S. M. Smith et al.)) was then used to associate multiple behavioral measures (tasks and scales) with the connectivity properties of structural brain networks across age (Rubinov and Sporns; Bassett and Sporns). A single

CCA axis of covariation successfully mapped brain networks to behavioral features. Critically, the CCA axis was associated with the individual participants' age indicating that a coherent pattern of degradation affects both brain networks and behavior. Finally, representational similarity analysis (Diedrichsen and Kriegeskorte) applied to the cross-validated CCA factors determined which global factors in multiple brain networks (Yeo et al.) and behavioral domains (Shafto et al.) jointly associated with predicting age.

Results

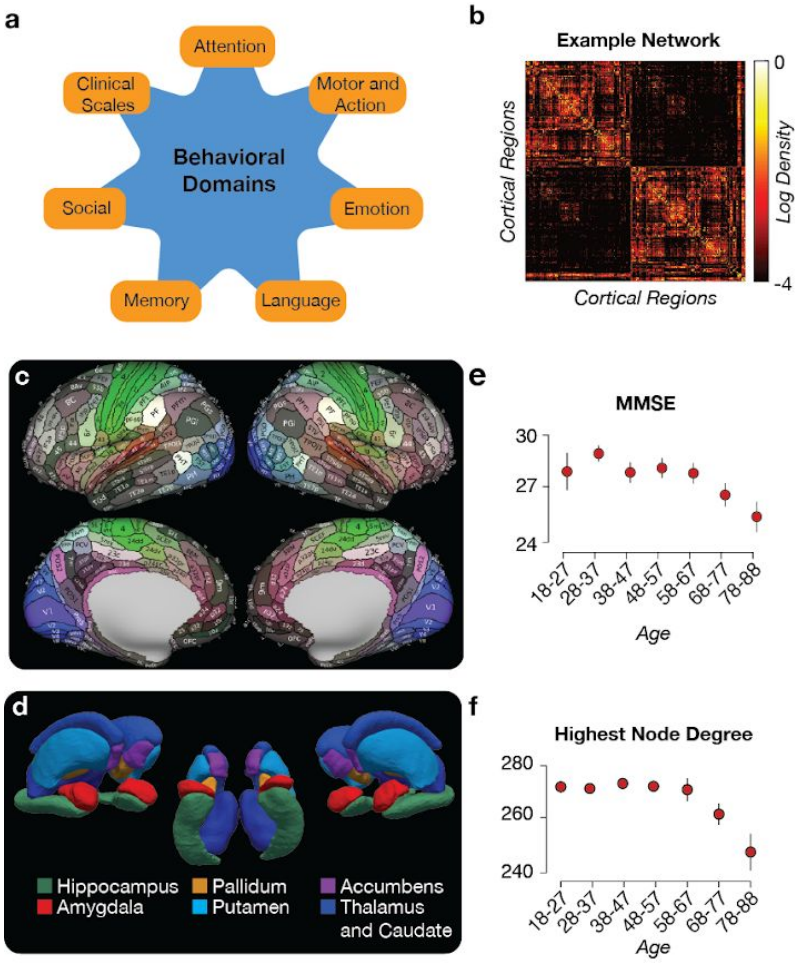

Figure 1. Main Findings. a. The behavioral domains. A simple graphic displaying the different behavioral domain labels is displayed. **b. An example network.** This is an example of an individual's network that is created for analysis. Each row and column represents a cortical region while the color represents the log scale of the density of the connection between nodes (weaker connections are black, stronger connections are yellow). **c. The cortical regions used to create the network structures.** This figure, taken from Glasser et al. (2016), represents the cortical labels used to construct the network in **b**. **d. Additional subcortical labels.** A surface rendering of the subcortical labels that were estimated and added to the cortical labels shown in **e. Trends in behavior over the lifespan.** The mean and standard deviation for the Mini-Mental State Exam (MMSE) is binned into decades and is displayed. Error bars represent 2 units of standard error. **f. Trends in the connectome over the lifespan.** The mean and standard deviation for the highest node degree is binned into decades and is displayed. Error bars represent 2 units of standard error. Subjects were binned by decades starting at 18 years of Age (see (Shafto et al.)).

The goal was to estimate if the structural connectivity properties of human brain networks are associated with human behavior measured from tasks, questionnaires, and scales collected across the lifespan (18-88 years, Supplemental Figure 1). To do so, data from the Cambridge center for Ageing and Neuroscience was used, the dataset is hereafter referred to as CAN (Shafto et al.). The CAN dataset contains a deeply phenotyped cohort of cognitively healthy individuals (594 used here; See **Methods** for inclusion criteria) evenly sampled across the lifespan (100 subjects per decade). We used 388 behavioral scores from 33 assessments published with the CAN dataset. These scores consisted of either reaction times, accuracy, or performance scales–see example histograms of each type of score plotted across age are shown in **Figure 1a** and **Supplemental Figure 1**. A total of 334 normalized behavioral measures were extracted and utilized for all subsequent analyses (140 reaction-time, 188 accuracy, and 6 assessments; see **Methods: Performing the CCA**). The CAN behavioral measures were originally mapped into five behavioral domains (Shafto et al.): attention, language, memory, motor, and emotion. In addition to these, scores from social and clinical assessments were organized into two additional domains for a total of 7 behavioral domains (**Figure 1a**).

Whole-brain structural networks were estimated using diffusion-weighted magnetic resonance imaging (dMRI) data from 594 subjects (Shafto et al.). Neuroimaging data was processed using an automated and reproducible pipeline using brainlife.io (see **Table 1**; (Avesani et al.)). **Figure 1** panels **b-d** show a representative network, as well as the cortical (MMP v1.0; (Glasser et al.)) and subcortical (Patenaude et al.) atlases used for network neuroscience data generation. A total of 376

regions (366 cortical and 10 subcortical) were used to generate each network. The dMRI data was processed for artifacts removal and fiber model fitting using a recent robust method (see (Ades-Aron et al.) and bl.app.68). Whole-brain tractograms were generated using a novel pipeline called Reproducible Anatomically Constrained Ensemble Tracking (RACE-Track; see bl.app.101), which integrates two established methods (Takemura et al.; R. E. Smith et al.). RACE-Track tractograms were combined with the regions of interest from the two atlases (see bl.app.23) to build individual subjects' connectivity matrices. Connections present in less than half of the subjects were eliminated (see also **Supplemental Figure 2a**; (Roberts et al.)). Connection density (C_d, see *Eq. 1,* **Figure 1b,** generated by web service bl.app.121; (Cheng et al.)) was used as network edge weight. The 70,500 C_d estimates were reduced to 376 node degree estimates used for all subsequent analyses (see **Supplemental Figure 2a** (Rubinov and Sporns)).

Changes in network neuroscience and behavioral measures across the lifespan

The relationship between networks' node degree and performance in behavioral tasks and assessments was explored across the lifespan (**Figure 1e**, **f** and **Supplemental Figure 1**). The goal was to ensure replication of known trends established in the literature (Salthouse, *Theoretical Perspectives on Cognitive Aging*; Singanamalli et al.; Salat et al.; Davis et al.; Salthouse, "Neuroanatomical Substrates of Age-Related Cognitive Decline"; Q. Li et al.; Salthouse, "Trajectories of Normal Cognitive Aging"; Bajaj et al.; Rutter et al.; Oschwald et al.; Deary et al.; Craik and Bialystok; Cox et al.; Paxton et al.; Kong et al.; Zuo et al.; Salthouse, "What and When of Cognitive Aging"; Cole and Franke; Westlye et al.; Shafto et al.). Changes in both network and behavioral measures were observed – especially starting at the fourth-decade **Figure 1e, f** (Yeatman et al.).

A large subset of behavioral measures varied as a function of age (**Figure 1** and **Supplemental Figure 1**). Reaction times increased with age, accuracy decreased, and performance in multiple scales either decreased or increased with age depending on the scale valence ((Folstein; Folstein et al.); **Supplemental Figure 1a**). For example, reaction-time increased in the Force Matching Task, but accuracy decreased (**Supplemental Figure 1a**), performance in the Mini-Mental State Exam (MMSE) also decreased (**Supplemental Figure 1a**; (Shafto et al.)). To approximate these trends we fit a quadratic polynomial to each behavioral measure. We found that 166 of the total 334 behavioral variables increased with age (quadratic term: 0.034 ± 0.083 s.d., R^2 = 0.957 ± 0.123 s.d., AICc = 49.067 ± 4.977 s.d.), and the remaining 168 decreased with age (quadratic term: -0.005 ± 0.016 s.d., R^2 = 0.988 ± 0.050 s.d., AICc = 48.232 ± 1.079 s.d.).

To evaluate whether the brain networks generated using RACE-Track showed sensible changes in properties across the lifespan, we estimated the highest node degree (**Figure 1f** and we observed similar patterns when evaluating network density and efficiency see **Supplemental Figure 1b**). To summarize the effect of age on these three measures, we fit a quadratic polynomial. The highest network node degree was well described by a negative quadratic term; it increased early and decreased later in life (quadratic term: -0.005 ± 0.008 s.d., R^2 = 0.9996 ± 0.0004 s.d., AICc = 48.007 ± 0.007 s.d.; network density and efficiency demonstrated a similar negative quadratic pattern, **Supplemental Fig 1b**, *right*).

A single-mode of covariation relates structural networks and behavior and subjects age.

After replicating the established quadratic trends in brain and network properties and behavioral variables with age, we set out to build a model that would linearly associate all the measurements from the two data domains – brain and behavior. We did this because we wanted to determine whether a linear association well approximated the relationship between brain networks and behaviors. To do so we used canonical correlation analysis (CCA; (S. M. Smith et al.)). CCA finds the linear combination of variables that best associates measures from the two data domains across subjects. In the following analyses, CCA found the best linear combination of 376 brain network properties and 334 behavioral measures (see **Figure 2**, **Methods**, and **Supplemental Figure 2a**, **b** and **c**). To do so, the behavioral measures and networks' node degree estimated in each subject were organized into two matrices (D_1 and D_2; **Supplementary Figure 2a**). Confounding variables such as sex, handedness, height, body weight, heart rate, and blood pressure were regressed out from both D_1 and D_2 (see **Supplementary Figure 2a**, **Methods,** and (S. M. Smith et al.)). The eigenvector matrices (E_1 and E_2) estimated from D_1 and D_2 via Principal Component Analysis (PCA) were used as inputs to CCA ((S. M. Smith et al.); **Supplemental Figure 2b** and **c**). CCA found the weights (*a* and *b*) and canonical factors (F_1 and F_2) that best approximated E_1 and E_2 (**Supplemental Figure 2c** and **d**).

A first CCA model (M_0) used a large number of PCA eigenvectors (100) as inputs and no cross-validation to evaluate the best possible fitting model to the data (S. M. Smith et al.). M_0 returned multiple large and statistically significant modes of covariation explaining the relationship on the first canonical axis (CA_1) between networks and behaviors (CA_1=0.860-0.1072; $p_{1\text{-}75}$=0.000 and $p_{76\text{-}85}$<0.01 bootstrap test). After this exploratory model, a 5-fold cross-validation approach (subjects as a random variable; **Supplementary Figure 2e**) was used to further test axis association between networks and behavioral

variables. A grid-search approach was used to generate 9,801 CCA models with different combinations of PCA numbers (spanning from 2 to 100). Each model was cross-validated using 15,000 5-fold throws for a total of 147,015,000 tested models. The first canonical correlation for a majority of these models was large with a mean CA_1 of 0.5468±0.09 s.d. (min and max 0.235 and 0.604, respectively). Over 90% of the CA_1 values across all models lay above 0.55, this indicated that, with a few exceptions, a majority of the cross-validated models CA_1 explained the data reasonably well.

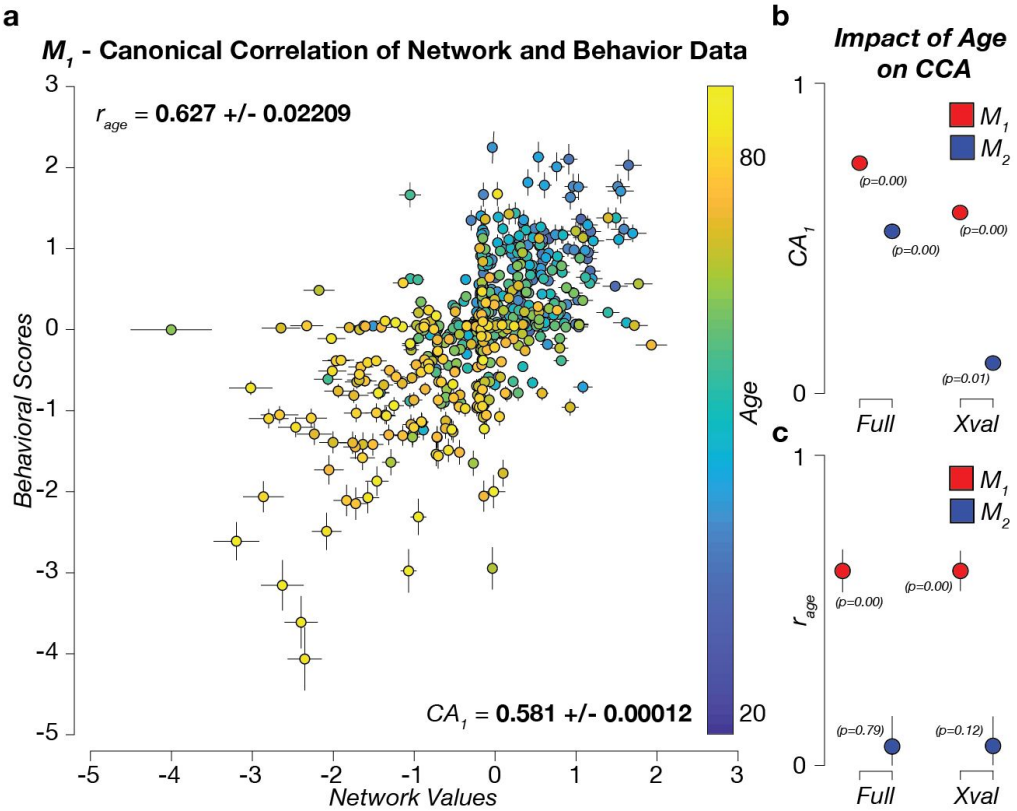

Figure 2. Human age explains the majority of the variability in the linear association between brain networks and behavioral variables. a. The first canonical axis (CA_1) from the cross-validated model (M_1). Each point represents a subject's cross-validated factor score on the brain and behavior axes, respectively. Error bars represent ±3 Standard Error of the Mean (SEM). The color of each point represents the age of the subject. The labeled correlations refer to the correlation of age to the combined canonical axis (r_{age}; *top*) and the correlation between the two canonical axes (CA_1; *bottom*) ±3 SEM**. b.** Association between the brain network and behavior data for the first canonical axis (CA_1) shown for both M_1 and M_2. Note the reported ±3 SEM are smaller than the symbols. **c.** Association (r_{age}) between the data in the first canonical axis (CA_1) and each participant's age. Error bars show ±3 SEM. Statistical significance estimated with bootstrap test reporting the p-value directly instead of relying on an arbitrary threshold.

Because of the established association between age and several brain and behavioral measures (see **Figure 1**), we selected the model (M_1) with the highest correlation between age and CA_1 (r_{age}=0.627±0.02209). r_{age} was computed using a multiway correlation via a general linear model where subjects' age was predicted using $CA_{1,behavior}$, and $CA_{1,network}$ as regressors (see **Methods**, *Eq. 3*). The selected model, M_1, had 38 brain and 40 behavior principal components and a significant CA_1 of 0.581±0.0001 (p=0.000 bootstrap test). Noticeably, CA_1 was the only significant mode in M_1 (see **Figure 2a** and **b**, see also **Methods** and **Supplemental Figure 2f-h**). The remaining modes were either not statistically significant (average $CA_{3\text{-}38}$=0.004±0.014; p=0.442±0.254 s.d. bootstrap test) or had no statistically significant loadings (CA_2; see **Supplemental Figure 2i** and **j** and next section). r_{age} was strong and statistically significant for the first mode as expected given the model selection procedure (0.627±0.022; p=0.000 bootstrap test) and not significant for the rest of modes (average r_{age} for $CA_{2\text{-}38}$ was 0.077±0.022; p=0.46±0.029 bootstrap test).

Two additional analyses we performed to further explore and validate the results. First, r_{age} was also computed for the exploratory mode, M_0. Also in this case the association was found to be significant for CA_1 only (r_{age}=0.611±0.023; p=0.000 bootstrap test; average $CA_{2\text{-}38}$, r_{age}=0.063±0.015; p=0.726±0.265 s.d. bootstrap test, see **Methods**). Finally, to validate the consistency of our approach, and the role of age in the association between brain networks and behaviors a new CCA model

was specified (M_2). M_2 was similar to M_1 with the exception that the subjects' age was regressed out from both the brain and behavior data before performing the PCA (See **Methods**, *Eq. 2*). CA_1 for M_2 was extremely small even though somehow significant (0.098±0.0016; p=0.007 bootstrap test). None of the remaining modes for M_2 were significant (average $CA_{2\text{-}38}$, 0.0003±0.017; p=0.520±0.290 s.d. bootstrap test; see **Supplemental Figure 2k, l**). As expected, the correlation between age and $CA_{1\text{-}38}$ for M_2 was insignificant (average r_{age}=0.075±0.019 s.d. and p=0.490±0.300 s.d. bootstrap test). In sum, the entirety of these results show that a large portion of the variance in the linear combination between brain and behavioral variables in the dataset can be accounted for by the subjects' age.

Brain network and behavioral components contributing to predicting age.

We further investigated the behavioral domains and brain networks nodes that most contributed to M_1, and indirectly to the predominant association with the subject age. To do so, the CCA variable loadings, L_1 and L_2 were estimated by computing the correlation between each column in D_1 and D_2 and every column in F_1 and F_2, respectively (**Supplementary Figure 3a**; (S. M. Smith et al.)). The top 20 L_1 and L_2 are reported for CA_1 (**Figure 3a** and **b** for brain networks and behavior respectively). The results show that the brain network nodes known to be affected by aging were among the top contributors (Samanez-Larkin et al.; Gutchess). This is the case for the hippocampus and the thalamus, which both returned high loadings. In parallel, behavioral tasks and scales measuring cognitive and emotional domains also known to be affected during human aging returned meaningful loadings as well (Park and Reuter-Lorenz; Oschwald et al.). These domains consisted of visual recognition, attention, and memory tasks, as well as, reasoning and language comprehension scales. No significant canonical loadings were found for $CA_{2\text{-}38}$ (see **Supplemental Figure 3b** for CA_2 loadings). For completeness, we also tested all the loadings for cross validated M_2. No significant loading was found for this model (see **Supplemental Figure 3c** p>0.05 bootstrap test). In sum, none of the CA in M_2 was interpretable, hence the model was uninterpretable.

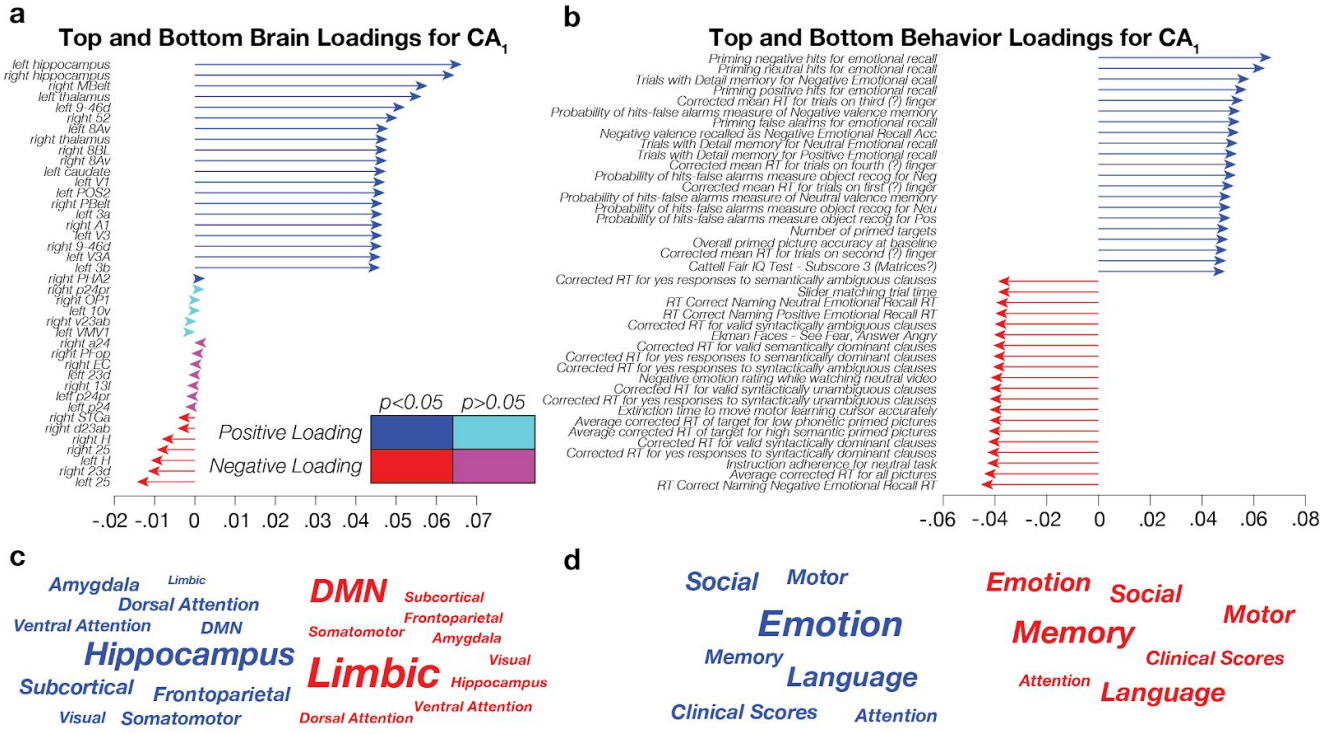

Figure 3. Top contribution brain network nodes and behavioral variables to the canonical correlation analysis (CCA loadings). a. The highest and lowest contributing cortical nodes within the network. The loadings for the brain regions are sorted by strength, with the highest and lowest 20 presented. The length of the line represents the magnitude of the loading. Significant loadings are either blue or red, depending on whether the factors are positive or negative, respectively. Non-significant loadings are presented in cyan or magenta. **b. The highest and lowest contributing behavior scores within the domain.** The loadings for the behavior scores are sorted by strength, with the highest and lowest 20 presented. The length of the line represents the magnitude of the loading. **c. Word cloud of brain network contributions.** Each label of the brain networks is used to summarize the nodes that are scaled to represent the average contribution of CCA loadings within the network. The larger the font, the greater the contribution to the respective network to the factor. The contributions to the positive axis are represented in blue (*left*) and the contributions to the negative axis are presented in red (*right*). **d. Word cloud of behavior domain contributions.** Each label of the behavior domain is used to summarize the nodes and is scaled to represent the average contribution of CCA loadings within the behavior domain. The larger the font, the greater the contribution to the respective domain to the factor. The contributions to the positive axis are presented in blue (*left*) and those to the negative axis in red (*right*).

To summarize the top contributors to M_1, word-cloud representations of the variable domains were created (**Figure 3c** and **d**). The word-cloud for the brain network loadings was built by assigning the labels from the Glasser atlas to a set of established functional network labels (Yeo et al.), hereafter referred to as Y_{2011}. Each of the 376 nodes in our networks was assigned to one of the seven functional networks in Y_{2011}; Visual, Somatomotor, Limbic, Ventral attention, Dorsal Attention, Frontoparietal, Default Mode (DMN; see **Methods** for the assignment of the networks nodes to major functional networks in Y_{2011}). In addition, the hippocampus, amygdala were kept separated and all the remaining subcortical structures were combined and reported as subcortical (i.e., pallidum, putamen, accumbens, thalamus, and caudate). This process generated a total of ten words (or clusters). Each word was scaled by the sum of the loadings of all the nodes assigned to the cluster (**Figure 3c,** see also **Methods** for a description of how the word-clouds were generated from the loadings).

This analysis highlighted the top functional networks and subcortical structures contributing to M_1, the one that indirectly also contributed to predicting the subjects' age. The limbic and default-mode networks, and the hippocampus returned the strongest contribution (positive and negative, respectively). Other networks, such as the frontoparietal and dorsal attention, as well as the amygdala provided a strong positive contribution. A similar, word-cloud representation was implemented also for the behavioral variables. Each of the 334 tasks and scales was uniquely assigned to one of the seven behavioral domains described in **Figure 1a.** Their loadings were then averaged across all tasks and scales within each domain (**Figure 3d**). The word-cloud summary representation for the behavioral loadings shows the variables in the emotional, language, and memory domains contributed the most to M_1. Other variables such as social, attention, motor, and clinical scores provided secondary contributions.

The multivariate relationships between networks and behaviors.

Finally, representational similarity analysis (RSA; (Diedrichsen and Kriegeskorte; Kriegeskorte) was used to clarify the multivariate associations between behavioral domains and brain networks. The assumptions of this analysis are: (a) the CCA variables loadings contain a fingerprint of the multivariate associations of the brain and behavioral variables; (b) the fingerprint can be extracted by modeling the data with and without letting the age of the subjects contribute to the CCA model. To approach this goal, the CCA variables loadings (L_1 and L_2) were used as inputs to a RSA. RSA typically quantifies the dissimilarity between variables from two data domains; for example, brain function and behavioral performance (Kriegeskorte; Diedrichsen and Kriegeskorte). In our application instead of using the normalized data directly, we used the loadings measured for each variable via CCA. This allowed us to model (1) the brain network-to-network similarity, (2) the behavior-to-behavior similarity, and (3) the brain network-to-behavior similarity (**Supplemental Figure 4a**). Every variable loading in M_1 (376 network and 334 behavior variables) was correlated with the loadings of all the remaining variables in the model. This generated a square, positive-symmetric matrix (S_1) of size 710 (**Supplemental Figure 4c**, *top*). Each entry in S_1 contained a dissimilarity estimate between the loadings of every variable estimated in the CCA (*Eq. 4*). This approach leverages the inherent structure of the data captured by the CCA model and further explores how the loadings of each brain and behavior variable are associated amongst themselves.

The approach in turn allowed us to evidence contributions of each variable to multiple other variables simultaneously and visualize complex interactions between variables. For example, a low dissimilarity between the loadings of two variables would indicate that the two variables contribute coherently to the CCA factors. Conversely, a high dissimilarity between two variable loadings would indicate that the variables contribute differently to the CCA. Because the CCA factors within each data domain (brain or behavior) are organized in descending order, the correlation within a single data domain is expected to be larger than that between data domains. S_1 allowed us to capture the coherence among the loadings of the variables and explore the cross-domain associations contributing to the CCA model. Furthermore, because S_1 was constructed using model M_1, in which the majority of the variance was explained by subject's age (see **Figure 2** and associated text), it was assumed that S_1 also depended on subject age.

To summarize the results in S_1, the brain network nodes and behavioral variables were mapped to the 10 brain networks and 7 behavioral domains of Y_{2011} (as described in the previous section). The dissimilarity values from network nodes and behavioral variables assigned to each domain were averaged to reduce the dimensionality of the dissimilarity matrix from 251,695 (upper diagonal of the original 710^2 matrices) to 136 (upper diagonal of the 17^2 matrices; see **Supplementary Figure 4d**). After that, the analysis focussed on dissimilarity between brain networks and behavior was emphasized (**Supplementary Figure 4e**). The results were visualized using a modified chord plot (**Supplementary Figure 4e**; see **Methods**). The chord plot allowed us

to show how multiple associations between brain and behavior load into M_1 simultaneously (**Supplementary Figure 4f**). It is convenient to describe the results in S_1 by taking the perspective of the behavioral domains and look at how each domain was associated with the various brain network domains.

Results show that memory, language, emotion, and attention dominated the association with the brain networks over clinical scores, motor, and social variables (compare the chord edge size in **Supplementary Figure 4f**). In the brain network domains, the frontoparietal, amygdala, hippocampus, subcortical, and dorsal attention domains dominated S_1. Next, the influence of subjects' age was evaluated more specifically by computing the RSA using M_2. A dissimilarity matrix S_2 was computed repeating the procedure explained above and then S_1 and S_2 compared.

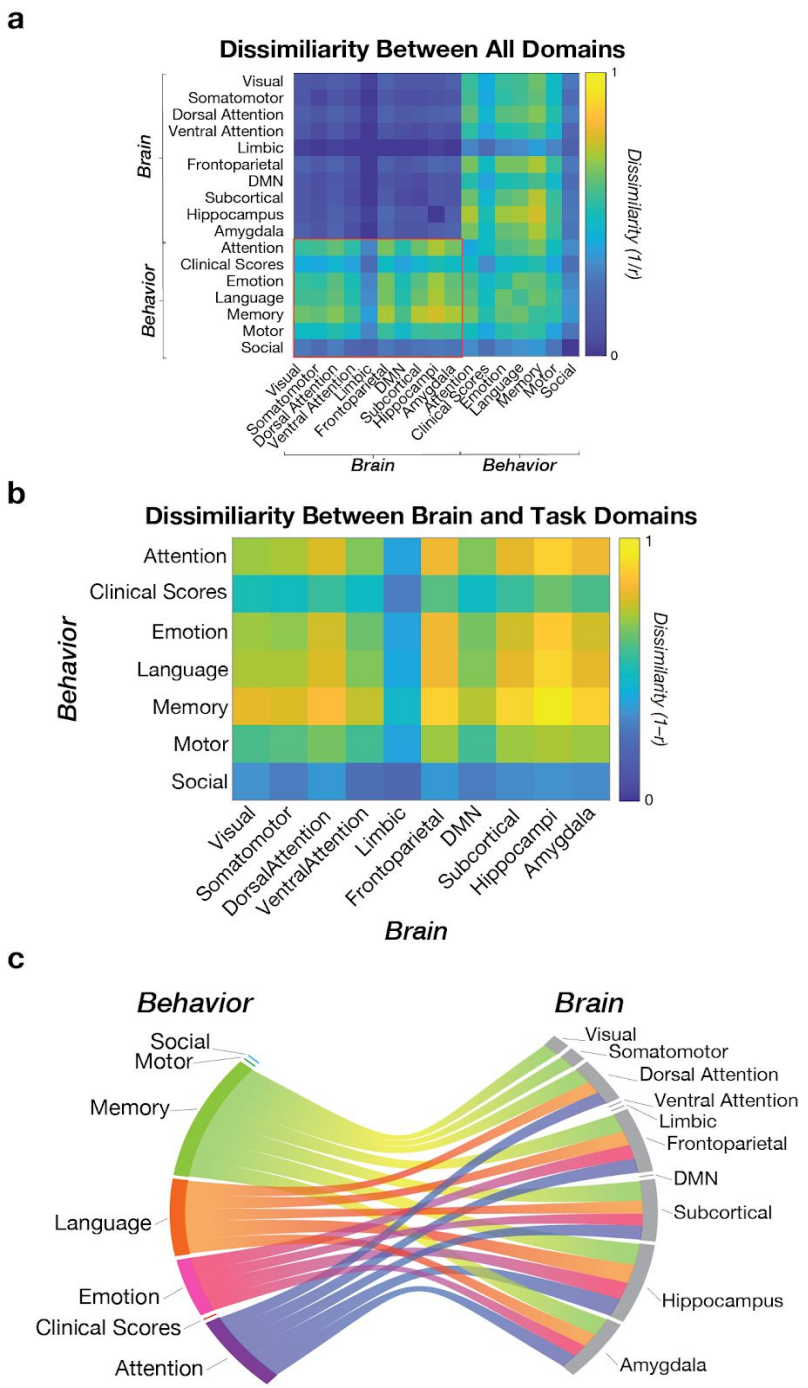

Figure 4. Representational Similarity Analysis of the associations between structural connectivity and behavioral domains.

a. The contribution of age to the RSA. The values in the matrix represent the dissimilarity between any pair of modules. A higher value means the modules interact more independently. These values represent the difference between the CCA models M_1 (when age is unaccounted for) and M_2 (when age is regressed out). The difference between the RSA matrices of M_1 (S_1) and M_2 (S_2) is the difference in dissimilarity age accounts for within these relationships (S_d). The red rectangle represents the subset of brain-behavior interactions emphasized in **b**.

b. Emphasis on the impact of age on the recovered brain-behavior interactions. The data in panel **b** is a cropped part of panel **a**, emphasized in red. This subset of dissimilarity between brain and behavior domains represents the impact age has on the relationship between connectivity within the network modules and the behavioral domains. The CCA analysis scaled variables across both datasets to maximize a correlation independent of assumptions for how these datasets may interact. The RSA allows us to recover how the domains interact and evaluate if the factors estimated by the CCA are reasonable. The difference between S_1 and S_2 is the impact of age on the dissimilarity measures between the models (S_d).

c. A modified chord plot of the strongest association (*r*) between brain networks and behavioral domains. This modified chord plot represents the strength between the behavior domains and brain networks. Any connections below the 75th percentile are removed to emphasize the strongest connections. The thicker the chord between a behavior and brain domain, the greater influence age has. The larger the blue band the greater the impact of age on how that behavior domain interacts with the brain networks, or vice-versa.

To compare S_1 and S_2, brain network nodes and behavioral variables were mapped to the 10 brain networks and 7 behavioral domains of Y_{2011}. After that, the difference in dissimilarity between the corresponding networks and domains was computed $S_1 - S_2$ (S_d; **Figure 4a**, see also **Supplemental Figure 4c-f**). The matrix, S_d, evidences the dissimilarity values that are related to age but not to the rest of the variables because any common dissimilarity was subtracted out. S_d can be divided into three primary regions; brain network-to-network (*ntn*), behavior-to-behavior (*btb*), and behavior-to-network (*btn*). Because the interest here was to capture the unique relationship between brain and behavioral variables, *btn* was the focus of all the following analyses (**Figure 4a** red square and **Figure 4b**). The *btn* showed the relationships between brain and behavior loadings affected by the subject age. A chord plot was used to elucidate this relationship (**Figure 4c, Supplemental Table 1**). Three aspects of the chord plot are noted. First, the size of the wedges for each data domain reports the total impact of age on each domain to the analysis. Second, the size of the connections between the different domains shows the impact of age on the data domains. Third, the number of connections from each behavioral domain to each brain network informs us of the multivariate contributions of each network to the various behaviors.

Consistent with previous reports, the behavioral domains most affected by age were memory, language, emotion, and attention. Furthermore, each of the behavioral domains was associated with multiple brain networks, indicating a complex relationship among brain systems and human behavior across age. For example, the domain of emotion was associated through age with changes in the subcortical structures but also by the frontoparietal network, the hippocampus, and the amygdala. Similarly, attention was affected by the dorsal attention and frontoparietal network but also by the amygdala, hippocampus, and subcortical structures. Language and memory show a similar pattern. The previous analysis shows the multiple brain networks systems that meaningfully contribute to the variation in behavioral performance across age.

Discussion

Brain aging and disease have profound effects on society. Because of the increasing expected lifespan of the world population –many of us are living longer– it is increasingly important to understand how we can age healthily. Costs associated with an aging population are only expected to increase over the next few years, given the increase in life expectancy (1–5). In Europe, estimates reach up to 200 million individuals affected yearly, directly or via caregivers' networks. Such impact accounts for up to 800 billion euros in annual costs. For example, brain disease is likely to affect up to 25% of the European population and nearly 38% of the remaining global population. These numbers make understanding the brain and its relation to behavior paramount to the well being of society across the globe. Critical to this goal, is to increase our understanding of the normal variability across individuals in the large population is fundamental to improve the prodromal identification of individuals at risk versus individuals subject to normal aging (6–10). To address the need to capture human variability and aging at least three aspects of scientific inquiry will need to be addressed. First, more high-quality data will need to be connected to reach a population-level understanding of the human brain and behavior. Second, advanced computational approaches will need to be developed that can actually exploit the value of the data at the right scale. Finally, infrastructure will need to be in place to support large-scale computational analysis of thousands of individuals.

To understand aging we need large-scale, population-level studies. There is an increasing need to better understand the trajectory of healthy aging as a large portion of the world's population rapidly progresses into old age. The need to understand not only the expected course of senescence, but the interaction of brain structure and behavior will become increasingly important to understand the myriad of conditions that can impede independence later in life. Early open projects of this nature, such as the Alzheimer's Disease Neuroimaging Initiative (ADNI), have required large publicly available tools to facilitate the larger number of researchers who have analyzed factors related to ones in this dataset (Beaton et al.; Veitch et al.; Hao et al.; Rex et al.; Mueller et al.; Weiner et al.). More recent, large-scale population projects such as the Human Connectome Project, the ENIGMA Consortium, and the UK Biobank (Van Essen and Ugurbil; Thompson et al.; Cox et al.) have collected, organized, and openly distributed data to allow the implementation of data-driven neuroscience methods, mine novel findings, and build normative models of brain structure and function (Glasser et al.). These projects are already pursuing similar methods, and the presented analysis could easily be applied and extended to these datasets (S. M. Smith et al.; Tsvetanov et al.; Cox et al.; Falk et al.; Van Essen and Ugurbil).

To fully exploit large scale datasets advances in both computational methods and data-analysis infrastructure are needed. We described a multivariate analysis of a multimodal dataset (Shafto et al.). Multiple measures of brain structural connectivity and behavior were combined to estimate the impact of human age on multiple brain systems and behavioral domains. A model testing framework was developed using cross-validation to demonstrate a strong linear association between brain connectivity

and behaviors. The majority of the variance in the linear association between connectivity and behavior was accounted for by the first mode of the model. This model was selected to maximize the correlation with subject age. Data derivatives (<DOI to data record will be added upon publication>), code (https://github.com/bcmcpher/cca_aging) and reproducible cloud services (See **Table 1**) developed for the present work are made available for reuse by the wider scientific community. Finally, the RSA analysis showed a series of global patterns of association between the model, selected to maximize the correlation with the subjects' age, and that resemble findings reported when individual variables are measured individually.

We demonstrate that brain and behavior show multiple global changes across the human lifespans that go well beyond one-to-one correlations between a single brain system or behavioral task. Several previous studies inspired this work, providing ideas for the novel contributions produced in this study. Early work (S. M. Smith et al.) integrated functional brain networks and phenotypic data from a large dataset of healthy young adults (Van Essen and Ugurbil). A strong association between brain function and behavior was reported using canonical correlation analysis (CCA). Yet, age was not a significant result in the analysis as it was in ours, most likely due to the narrow age range in the Human Connectome Project sample used in that work compared to the CAN sample. Another relevant study used the CAN dataset, CCA, and generative models of brain functional activity and was first in reporting the effect of age on the association between cognitive performance and brain function (Tsvetanov et al.)). The study focused on three functional networks (Shirer et al.; Beckmann and Smith) and 6 composite measures of behavior and showed that neuronal, not vasculature-related effects in resting state networks are associated with age. A third relevant study was first in using brain structure (a multimodal combination of diffusion-measures and cortical partial volume estimates) to show an association with various demographics, including age (Llera et al.). The current results go beyond previous work by (1) thoroughly cross-validating the CCA, (2) testing how well a hold-out variable is predicted by the primary canonical axis, and (3) using an RSA on the variable loadings from the cross-validated model to recover relationships between the variables themselves. These improvements provide a way for future work to glean more insight from the increasingly large and multimodal samples of variables utilized in modern neuroscience. Furthermore, we created open services shared on brainlife.io to allow other researchers to freely process new data utilizing our pipeline.

As neuroscience shifts towards data-driven approaches, data-fusion methods (Dahne et al.; Silva et al.; Lydon-Staley et al.) such as CCA are likely to increase in popularity. Yet, the CCA approach used here is limited to two domains at a time. Other methods allow fusion across a higher number of data domains. For example, CCA has been generalized to higher-order models beyond 2 domains, similar to variations of Independent Component Analysis (joint- or linked-ICA; (Vince D. Calhoun et al.; Allen et al.; V. D. Calhoun et al.). Imaging genetics is one of the fastest growing fields that are capitalizing the most on methods such as CCA especially requiring to combine multiple data domains (Risacher and Saykin; Veitch et al.; Du et al.; Hao et al.; Thompson et al.; Hawrylycz et al.). These studies typically look at thousands of genetic markers from a single blood assay, similar to how a single MRI imaging session can be used to generate thousands of measures of brain structure and function. The benefit of methods such as CCA is due to the ability to model datasets with large numbers of variables from different domains (e.g. blood assays, behavior, genetics and neuroimaging). Yet, in addition to variations of CCA, ICA analyses have also been proposed to map across multiple variable domains, though Partial Least Squares (PLS; (McIntosh and Mišić; Krishnan et al.; McIntosh and Lobaugh)) is perhaps the most common approach that allows mapping the combination of multiple data modalities into a single space (Bijsterbosch et al.; Bae et al.). Furthermore, the current work is also limited to linear interactions between data domains. Future explorations of the multivariate interactions might contribute additional novel insights (Wang et al.; Marek et al.). Nonlinear interactions estimated through kernel embedding (Helmer et al.) or structural equation modelling (Mueller and Hancock) are particularly promising, but have not yet been applied to datasets similar to the one used here. Critically, one recent report has sparked interest by suggesting that adding nonlinear interactions to data modelling may provide negligible improvement over linear models when comparing brain-behavior interactions (Schulz et al.). In selecting the best models (linear or nonlinear) might also depend on data preprocessing (Assem et al.; Hsu and Culhane). The effectiveness of data preprocessing may vary depending on the characteristics of the data domains. Future work will be required to determine what data domains will require linear or non-linear modelling approaches.

As neuroscience moves to population-level neuroscience, reproducible approaches to data management and analysis need to be embraced. Sharing data products is essential to implementing transparent, replicable, and reproducible brain research (23). Critical to the success of the next generation large-scale neuroscience methods will be to embrace new technology to ensure results reproducibility. This will require embracing methods for open science, data, and computational standards as well as modern computing infrastructure to lower the barriers of entry to proficient large-scale data methods (24–26). Our study follows up on the most recent trends in terms of large-scale datasets and computational approaches. But also the study is the

first to embrace the most recent technology to support scientific reproducibility to clarify human aging. We used the recently developed, community-developed, and publicly-funded cloud computing platforms, brainlife.io. brainlife.io allows processing large amounts of data by tracking the provenance of each dataset and by linking the data-object on the platform with the reproducible web-services used to generate the data. brainlife.io addresses precisely the needs for replicability and reproducibility highlighted by the recent report by the U.S. National Academies (23). Indeed, to implement our study we developed more than ten new data analyses applications that are now available on brainlife.io for other investigators to reuse for new research or to replicate our results.

Methods

Data source. The behavior and neuroimaging data were accessed from the publicly distributed Cambridge center for Ageing and Neuroscience (CAN) dataset (Shafto et al.). This large dataset provides cross-sectional data on 652 individuals. Of this total 623 had imaging data of interest to the current study (diffusion-weighted MRI and T1-weighted MRI). Out of a total of 623 individuals, 594 neuroimaging datasets were successfully processed and included in this present study. Quality control issues on the processed T1w data (FreeSurfer did not successfully segment the brain) motivated the exclusion of 26 subjects. **Supplemental Figure 2a** shows the dimensionality of the data (*n*=594).

Behavioral data. Participants responded to a series of screening and demographic questionnaires and performed behavioral tasks and clinical tests (Shafto et al.). See (Shafto et al.) for details on the tasks, tests and questionnaires. A total of 1,708 measurements per individual were acquired by the CAN consortium. Only behavior scores normalized by the CAN consortium were utilized for the current study, as a result, a total of 388 CAN-normalized scores were utilized for further analysis. All these measurements were initially subdivided into five of the primary behavioral domains: attention, memory, language, emotion, and motor (Shafto et al.). For the current study, in addition to the five original behavioral domains, test scores collected by the CAN consortium measuring social engagement and clinical scores were also utilized and collected into a Social and Clinical behavioral domain for a total of 7 domains (**Figure 1a**). The social engagement measures consisted of 10 questions related to the frequency and mode of socialization of the individuals. Six clinical questionnaires were collected into the clinical domain: the MMSE, ACE-R, Wechsler Memory test, “Spot the Word”, the Cambridge 10MQ, and the PSQI Sleep Index (Yeo et al.; Shafto et al.).

Neuroimaging Data Preprocessing.

Anatomical MRI data preprocessing. A T1w and T2w anatomical scans were acquired for each individual. Both scans have a 1mm isotropic resolution (T1w: 3D MPRAGE, TR=2250ms, TE=2.99ms, TI=900ms; FA=9 deg; FOV=256x240x192mm; GRAPPA=2; TA=4mins 32s. T2w: 3D SPACE, TR=2800ms, TE=408ms, TI=900ms; FOV=256x256x192mm; GRAPPA=2; TA=4mins 30s). Both images were reoriented and aligned to the AC-PC plane with a 6 degree of freedom rigid alignment to the MNI template based on the Human Connectome Project (HCP) procedure (T1 reorientation; bl.app.15, T2 reorientation; brainlife.app.114, T1 alignment; bl.app.99, T2 alignment; brainlife.app.116). These AC-PC aligned images were passed to Freesurfer 6.0 (Fischl), which reconstructs the white matter and pial surface based on the T1 image, using the T2 image for additional information to better estimate the surfaces (FreeSurfer; bl.app.0). The FreeSurfer output was used by the multi-atlas transfer tool (maTT; bl.app.23) to align individual subjects T1w anatomy files to the multimodal cortical brain atlas (MMP v1.0 Atlas (Glasser et al.). The labels from the MMP atlas were used to build networks, see below.

Diffusion-weighted MRI data preprocessing. The diffusion-weighted MRI data (dMRI) contained a total of 60 directions collected across 2 b-value gradients (2D twice-refocused SE EPI, TR=9100ms, TE=104ms, TI=900ms; FOV=192x192mm; 66 axial slices, 2 mm isotropic; B0=0,1000/2000s/mm^2, 30 unique directions per shell; TA=10mins 2s. Readout time 0.0684; echo spacing=0.72ms, EPI factor=96). Data were processed using MRtrix3 (bl.app.68; (Ades-Aron et al.; Tournier et al.). The following are the steps of the preprocessing procedure. The diffusion gradient alignment to the data was checked using a simple tracking procedure to find the orientation that produces the longest streamlines. After that, a PCA denoising procedure was performed to remove scanner noise not associated with the diffusion signal. Gibbs ringing, Eddy currents, inhomogeneity, and motion artifacts correction was performed. After all previous steps, an additional Rician-denoising was performed. The mean B0 image across (2 repeats) was extracted and utilized to register the dMRI to the AC-PC aligned T1-weighted image using Boundary Based Registration (BBR, (Greve and Fischl)). The diffusion-weighting gradients were rotated to account for motion correction and AC-PC alignment. Finally, the diffusion-weighted image was resampled to a 1 mm isotropic.

Tractography generation. We developed an automated cloud computing service that we call Reproducible Anatomically Constrained Ensemble Tracking (RACE-Track; bl.app.101). RACE-Track combines Anatomically constrained tracking (R. E. Smith et al.) with ensemble methods (Takemura et al.) and is containerized for public, reproducible access on the open cloud computing platform brainlife.io (Avesani et al.). The preprocessed dMRI data was used to generate whole-brain tractography using RACE-Trac. Specifically, a constrained spherical deconvolution (CSD) response function was estimated for white matter, gray matter, and cerebrospinal fluid (CSF) as previously described (Jeurissen et al.; Tournier et al.). Each respective response function was then used to estimate Fiber Orientation Distribution (FOD) maps for each tissue type. Following the ET approach, we fit the CSD model using multiple L_{max} (2, 4, and 6), this procedure created three FOD maps one per L_{max}. The FOD maps

were then passed to the iFOD2 tracking algorithm as previously described (R. E. Smith et al.). The T1w image was used to separate the brain tissue into its five types: 1) corticospinal fluid, 2) white matter, 3) gray matter, 4) subcortical gray matter and 5) pathological tissue. The image probability maps generated for each tissue were used for initiating and stopping tractography. More specifically, the gray-matter-white-matter interface was used as a seed mask for the streamlines, this approach has been demonstrated to providing a more complete coverage of tractography terminations on the cortex and subcortical gray matter structures (R. E. Smith et al.). Furthermore, the whole tractography procedure was repeated for both deterministic and probabilistic tracking, across the three L_{max} and five different maximum angles of curvature (5, 10, 20, 40, and 80º). A total of 600,000 streamlines was generated in each individual using this tracking procedure.

Construction of structural brain networks. Whole brain structural brain networks were built utilizing the multimodal cortical brain atlas (MMP v1.0; (Glasser et al.)). The MMP atlas was aligned to individual subjects' brains with maTT (bl.app.23). The parcels of the MMP were used as nodes for the brain networks. The edges of the networks were defined as the density of connections between two parcels. Connection density was computed as the number of streamlines terminating in the two parcels divided by total number of voxels in the parcels (Cheng et al.):

$$C_d = (2 \cdot s_{i,j})/(n_i + n_j) \quad \text{Eq. 1}$$

Where C_d is the estimated streamline density for a connection (network edge), $s_{i,j}$ is the number of streamlines terminating in both regions, n_i and n_j are the number of voxels in each of the two brain regions. Networks matrices were created using Eq. 1 using a reproducible algorithm implemented on brainlife.io (bl.app.121). After that, the network matrices were thresholded by removing connections not present in at least half of the participants and then computing node degree for each individual network matrix using the Brain Connectivity Toolbox (Rubinov and Sporns).

App name	App purpose	DOI
AC-PC Alignment of T1	*Align T1w anatomical images along the AC-PC plane*	bl.app.99
AC-PC Alignment of T2	*Align T2w anatomical images along the AC-PC plane*	bl.app.116
FreeSurfer (v6.0.0)	*Create surfaces and cortical labels*	bl.app.0
dMRI Preprocessing	*Correct dMRI data of artifacts and align to T1w image*	bl.app.68
RACE-Track (Tractography)	*Create an anatomically constrained whole brain ensemble tractogram*	bl.app.101
Multi-Atlas Transfer Tool (maTT)	*Map MMP atlas to individual subjects' brains*	bl.app.23
Network Construction	*Create networks from tractography and cortical labels*	bl.app.121

Table 1. Open brainlife.io web services and containerized applications implementing the processing pipeline developed for the current work. We developed a computationally reproducible data processing pipeline utilizing the cloud computing platform brainlife.io (Avesani et al.). Each step within the pipeline is described in **Table 1** and available for download as Docker (Anderson) container run via Singularity (Kurtzer et al.). Each step of the pipeline is also publicly shared as an App (web service) on the brainlife.io platform. brainlife.io Apps can be freely executed on public or private computing resources. All processed brain imaging data and Apps are accessible in a single record as a brainlife.io publication at <<DOI-TO-MY-DATA>> (Avesani et al.).

Canonical correlation analysis and data preprocessing.

Behavior features. The total of 388 behavioral variables (m_1; **Supplemental Figure 2a**) were extracted from the CAN project. Data were prepared for modelling by applying a z-score transformation to each measurement across subjects (S. M. Smith et al.). Furthermore, variables with extreme outliers (more than three standard deviations from the population mean) or absent in at least half of subjects were eliminated from further analysis. Fifty-four of the behavioral variables were eliminated via normalization, bringing the total number of behavioral data utilized 388 to 334. These features were organized into a matrix (D_1) composed of all behavioral (594 subjects, n, and 334 behavioral variables, m_1). See **Supplemental Figure 2a** and **Equation 1**.

Network neuroscience features. Node degree was estimated using the streamline density networks generated described above for each subject (Rubinov and Sporns). This estimation procedure resulted in 376 node-degree measures per subject (m_2). The upper diagonal of each network was unwinded to create a vector of features 1x70,500 in size (S. M. Smith et al.). These features were organized into a matrix (D_2) composed of all brain data (594 subjects, n, and 70,500 node-degree estimates, m_2). See **Supplemental Figure 2a** and **Equation 1**.

Data normalization. Both the brain and behavior datasets were normalized through the same process. First, the datasets were normalized by removing the mean of each feature across subjects and dividing by the standard deviation across

subjects. Next, nuisance variables were regressed from each dataset to remove their influence on the data. These variables include a subjects' height, weight, gender, heart rate and systolic and diastolic blood pressure. Behavior data was also rotated to the nearest positive definite pairwise covariance matrix to better account for correlation between variables (S. M. Smith et al.). This step was not required and not performed on the brain network data. Principal component analysis (PCA) was performed on D_1 and D_2 separately to reduce the number of dimensions in the data. PCA generated two eigenvector matrices, E_1 and E_2, for D_1 and D_2, respectively (see **Supplemental Figure 2b** and **Equation 1**). Because the choice of number of principal components (PCs) is arbitrary, we explored a wide range of PCs (2-100) and selected the PC number for D_1 and D_2 that best predicted the individual subjects' age (see below for more details).

Canonical correlation analysis (CCA). We used E_1 and E_2 to perform canonical correlation analysis (see **Supplemental Figure 2c**). The CCA algorithm estimates the linear combination of variables from each dataset that maximizes the correlation between the datasets

$$\rho = max_{a,b}[Corr(a^T D_1, b^T D_2)] \quad \text{Eq. 2.}$$

where ρ is the correlation between the datasets being maximized, D_1 and D_2 are the normalized datasets, and a and b are the weighting matrices that linearly combine the data variables into the canonical scores . The CCA analysis returns two matrices, F_1 and F_2, containing the canonical factor scores for each subject to each of the estimated canonical factors. The factor scores describe how much each subject contributes to each of the latent factors. These factor scores are used plotting the canonical correlation axes, or canonical axes (CA, **Figure 2**, **Supplemental Figure 2**, red). We use the combination of the first factor scores from each dataset to estimate the correlation with age.

To better interpret the contribution of individual variables within the CCA factors, variable loadings are reconstructed from the normalized data and the canonical factors. The loading values, L_1 and L_2 for brain and behavior respectively, describe the strength of the variables contribution to the axis. The loading matrices' dimensions are the number of variables in the dataset by the number of estimated canonical factors. Each variable has a loading for every factor. The loadings are recovered for a variable by correlating the original normalized variables for every subject with the corresponding factor scores. This process is repeated and every variable is correlated with a factor to create the variable loadings for a canonical axis. By correlating the normalized variable observations (each column of matrix *D*) to each factor score (each column of matrix *F*) (**Supplemental Figure 2**) for every canonical factor estimated in both datasets, we generate canonical loadings (*L*) for every variable and every factor. For example, a specific behavioral score could be highly correlated with a canonical factor, indicating that the behavior is highly predictive of changes in this factor. When this is done for every axis, a complete matrix L of variable loadings is recovered. The highest variable loadings for a canonical axis indicate the variables that contribute most to the positive end of the canonical factor, while the lowest variable loadings indicate the variables that contribute most to the negative end of the canonical factor. This is reported in Figure 3. The variable loadings are the typical way of inspecting how variables within a CCA analysis interact.

Correlation with Age. To determine the association of a canonical axis with age, we used a multi-way correlation with the first canonical factors to determine an r coefficient between the canonical axis and age. Age was predicted by

$$age = CA_{1,network} w_1 + CA_{1,behavior} w_2 + b \quad \text{Eq. 3}$$

where age is the age of each subject, $CA_{1,\ network}$ is every subjects score in the first column of the brain factors (F_1), $CA_{1,behavior}$ is every subjects score in the first column of the behavior factors (F_2), w_1 and w_2 are the beta estimates of the model, and b is the intercept. This is an ordinary least squares linear regression using the canonical scores of the behavior and brain from the first factor predicting age. To determine the correlation between the factors and age, we take the square root of the R2 from the fit model to estimate the correlation coefficient between the combination of factors and age. This is equivalent to the correlation with age along the canonical axis of the estimated factors. To determine the significance of the correlation of age to the canonical axis, a bootstrap test of 10,000 permutations was performed by randomly sorting the rows with replacement of $CA_{1,\ network}$ and $CA_{1,behavior}$ to determine a null prediction. This allowed us to determine if the observed correlation with age was significantly different from zero. To estimate the standard error of the estimate, a separate 10,000 permutation bootstrap was estimated, sampling with replacement both factors and age. The resampled estimates of age were used to create a rempled mean and standard error of the correlation between the canonical factors and age.

Parameter tuning. The goal of this analysis is to maximize the correlation with age. However, the principal components analysis performed as part of the preparation of the data for the CCA will combine variables differently depending on the

number of components requested (**Supplemental Figure 2f**, **g**, **h**). Further, the number of PCA components indicates the number of canonical factors that can be estimated. Typically, a number such as 20 or 100 is selected by the researcher. However, there is reason to believe that the number of requested components will impact the final correlation with age (**Supplemental Figure 2f**, **g**, **h**). To test this we tuned the number of PCA components using a grid search, selecting the number of principal components based on the strength of the resulting correlation with age. This hyperparameter sweep found the correlation with age on the primary canonical factors for every combination of PCA components between 2 and 100 on the input datasets. See Supplemental Figure **2e, d** for the results from the search space. We selected 38 principal components for the brain axis and 40 principal components for the behavior axis because this combination of principal components resulted in CCA factors with the highest correlation with age. Nearby parameter spaces had similar levels of correlation with age. Importantly, the most common combinations of parameters, [20x20] and [100x100], had a significantly worse correlation with age than the model with the optimal parameters (**Supplemental Figure 2f**, **g**, **h**). This is further supported by inspecting the variable loadings of the models that performed worse than the tuned solution. The variable loadings in the suboptimal models had different combinations of variables as the strongest and weakest loadings. This difference indicates that the CCA used a different combination of variables to form the canonical factors in these models. These different factors are less effective at predicting age. This indicates that the selection of the number of principal components for this analysis is important in tuning an accurate model.

Model selection. All factors and loadings were cross-validated using a repeated 5-fold process to better ensure the generalizability of this model to the larger population (**Supplemental Figure 2e**). A repeated k-fold process is conceptually similar to a typical k-fold approach. A standard k-fold approach models data by training the parameters on a majority portion of the subjects and then applying the fit parameters to a holdout set of subjects to observe the generalizability of the trained parameters to new samples from the same population. The two key differences between the repeated k-fold process and a standard k-fold process is that 1) in a repeated k-fold process all observations end up with a held out estimate and 2) the training/test process is repeated many times to estimate a distribution of hold out parameters. The central tendency of the hold out parameter's distribution is taken for each of the subject factors and variable loadings. For example, a standard k-fold cross-validation would divide the subjects evenly into an 80-20 train/test split. The CCA would be fit, or trained, on 80% of the subjects. The trained parameters from 80% of the subjects would be applied to the 20% holdout. The canonical factors and variable loadings are compared between the train and test data to determine how well the model generalizes to the population.

To perform the repeated k-fold process, the dataset was first split into 5 equal groups of subjects. Then the CCA was fit 5 times using each combination of 4 of the groups to train the model, predicting the holdout estimates for each of the splits. This creates a full set of hold out estimates for every subject's factors (F) and loadings (L). This process is repeated 15,000 times, with each iteration creating a new random split of subjects into 5 groups before repeating the train/test procedure. This creates a distribution of trained factors and loadings for every parameter in the model. The median value of these distributions indicates the most probable trained value for the parameter. Additionally, the central tendency of these distributions is observed to quantify the standard error of the estimates. These median values of the permuted hold-out distributions are the factors and loadings used in evaluating the CCA (the factors values in Fig 1, the loading values in Fig 2). The repeated k-fold cross-validation approach allows the full dataset to be evaluated in the results, as each subject's factor scores and each variable's loadings are estimated from a model using unique observations to predict their estimate. This approach was necessary because the modeling of data with a CCA does not generalize to new observations well. The estimation of the CCA is based largely on deterministic matrix algebra, making the final results very sensitive to small perturbations in the input data. Selecting new training-test splits from the observations in a single k-fold cross-validation approach often resulted in different conclusions, while this repeated k-fold cross-validation consistently produces the same model estimates.

Additionally, this cross-validation approach is robust to our data being evenly sampled across our outcome of interest, age. Any one random sample of subjects from this dataset would be likely to bias the training or prediction of a particular age. Further, it is not possible to use age as part of the identification of training subjects while still being able to use it as an unbiased outcome. By cross-validating across many random k-fold splits we are able to cross-validate our model without risking an unintended bias with age that may be present in any one split.

Bootstrap Tests. A bootstrap method was used to test the statistical significance of the correlations and loadings within the CCA models (M_0, M_1 and M_2). For each of the various tests described in the results section, a null distribution was generated by resampling the data (or model parameters) with replacement. For each bootstrap test, 10,000 samples of the data (or

model parameters) were generated using the distribution of data (parameters). The bootstrap tests were implemented by assuming a null hypothesis of "no correlation between the two variables (or parameters)." Family-wise error estimates (FWE) of 0.01 was used as a cut-off on the null distribution. A correlation was reported as statistically significant if the *p* value of the correlation from the bootstrapped null distribution was found to be below 0.01. Gray shading in **Supplemental Figure 2i**, **j** show examples of the null distributions generated by bootstrap under the null hypothesis of no correlation between variables**.**

Representational Similarity Analysis (RSA)

We used Representational Similarity Analysis (RSA, (Diedrichsen and Kriegeskorte; Guntupalli et al.)) to create a fingerprint of how the loadings of the variables in one data domain (brain) are associated with the loadings of the variables in the other data domain (behavior)**.** We define factors as the estimated latent factors from the CCA analysis. The number of factors estimated is determined by the smallest number of tuned PCA parameters used during parameter tuning. Each variable has a loading for the factors estimated. We use a dissimilarity measure estimated between pairs of variable loadings to inspect how the variables interact with each other across all estimated factors. This allows us to observe how the individual observations within the domains of our CCA model, brain and behavior, interact with each other as they form the primary axes for all factors in the analysis. Typically, the extent of our inspection of the CCA model is using the cross-validated variable loadings ranked by their magnitude to indicate the strongest contributing variables from a particular domain (Fig 2). However, there is currently no way to recover how the individual variables interact with each other. While the CCA determines an overall interaction between the separate datasets and the variables that most contribute to each factor, there was previously no description of how the individual elements interact with one another in this model. Access to this information would prove particularly useful to determine what relationships within the data may be capitalized on to estimate the canonical factors, as there are many established brain-behavior interactions within this dataset.

The dissimilarity matrix (*S*) is positive and block symmetric, with three distinct components representing the network-to-network (*ntn*), behavior-to-behavior (*btb*) and brain-to-behavior (*btn*) dissimilarity. After building *S*, the elements of the matrix were sorted and organized into meaningful brain and behavioral domains. This organization allowed us to interpret values of *S* in terms of functional domains for both brain and behavior instead of individual regions or tasks. Multiple individual brain regions in $\mathcal{O}_{\mathrm{B}}$ were sorted and uniquely assigned into the Y_{2011} labels ((Yeo et al.); https://github.com/bcmcpher/cca_aging/blob/master/HCP_to_Yeo_assignment.tsv). The behavioral measurements in $\mathcal{O}_{\mathrm{b}}$ were mapped onto the seven major behavioral domains and averaged (Social, Emotional, Attention, Memory, Clinical, Language, and Motor). Results show that the CCA captures patterns of covariation between the two domains (brain and behavior). For example, the emotion domain is highly similar (low dissimilarity) both in the brain and behavior between the brain and behavioral contributions. Also, attention and memory are highly similar (low dissimilarity) as well. To contrast, these results to the normalized data, see **Supplemental Figure 4i-k** that shows the difference in range between the dissimilarity of the observed variables (x-axis) to the CCA estimates (y-axis).

To build the dissimilarity matrix between all variables used in the analysis, we first use the variable loadings reconstructed from the cross-validated factors. To construct the RSA, we take the dissimilarity measure between every pair of variables using their recovered loadings for all factors. This is taken across both L_1 and L_2 (the loading matrices for brain and behavior, respectively). Each row represents the canonical loadings for every canonical factor for the variable and each column is the order of the estimated canonical factors. By taking the dissimilarity measure between each row, we get a measure of how similarly any two variables behave across all the estimated factors. The dissimilarity is able to be taken across domains, meaning how the brain and behavior variables interact within their respective factors can be inspected directly.

The first factor of the CCA represents the factor structure of each domain that creates the strongest correlation between the datasets, while each subsequent factor represents the next orthogonal configuration that has the next strongest correlation. By comparing the variable loadings of each factor between two variables we can represent how the variables interact with each other across every estimated canonical factor. We use this full vector of estimated factor scores to determine the distance by calculating the dissimilarity between every unique pair of variables. A dissimilarity measure:

$$S_M = 1 - |\, corr_{x,y} \,| \quad \text{Eq. 4,}$$

where x and y are any pair of variable loadings in an [n x 1] vector. Each vector consists of the *n* loadings for each canonical factor estimated in the model for each variable. The correlation between these vectors would represent how similarly the variables contribute to each of the estimated canonical factors. Every unique combination of x and y created a symmetric matrix of size [710 x 710] with the respective dissimilarity value between every variable estimated. The values represent how

dissimilar any pair of variables behave across every estimated factor. The higher the score between the variables, the more independently they interact across all the estimated canonical factors. Likewise, the lower the score between the variables, the more similarly they behave across factors. To summarize this information, we sorted these measures into established behavior domains and brain networks. This better reveals how variables within a specific domain behave with variables from another domain. From this sorted matrix, we estimate the modules by averaging each value within a module into a single value. This creates a matrix of size [modules x modules] with the mean and standard deviation of dissimilarity values for every variable within that group. These values represent on average how the behavior domains and brain networks interact with each other across all the factors. However, the most important interactions for our purpose is the interaction between the brain-behavior averages, or how well the behavior domains correspond to the structural connectivity within established functional networks (**Figure 4e**).

To do so, we computed the loadings by correlating the original normalized data and the CCA factors for each canonical correlate estimated (columns of $D_{1,2}$ with columns of $F_{1,2}$, respectively). Two matrices were generated with this approach, one for the behavioral and one for the brain network loadings (L_1 and L_2). These loadings were then stacked into a matrix where each row is a variable and each column is the corresponding canonical axis (**Supplemental Figure 4a**) and used to compute the dissimilarity matrix between all brain regions and behavioral tasks. This creates a symmetric matrix where the pairwise dissimilarity distance between all rows of the stacked matrices was computed using Eq. 4 (**Figure 3a**; (Diedrichsen and Kriegeskorte)). The axes are the size of the number of variables included in the model and a value for each pair of variables indicating how similarly they behave across all canonical factors.

Chord Plot. To better visualize the association between brain and behavior we transformed the brain-behavior dissimilarity value back to correlations: $r = 1 - S_M$. These values were then used for a modified chord plot visualization. For this plot, the *r* values were normalized by rescaling them to better show the brain-behavior interactions. First, *r* was normalized between 0 and 1. Second, *r* values below the top 75th percentile were eliminated (**Supplementary Figure 4h-j**). Third, *r* was multiplied by 1,000 and squared to visually emphasize any difference in values. The chord plots represent the strength of the association between the CCA loadings of the brain networks and behavioral domains. Two aspects of this plot informa our analysis. (A) Each wedge of the chord shows the total association in a domain; the larger the wedge for a particular domain the larger the contribution to the CCA loadings. (B) The thicker the bands connecting a behavioral domain and a brain network, the stronger the association between the loadings in those variables.

Evidencing the effect of age to the CCA by computing the difference in RSA between M_1 and M_2. To determine the impact of age on the brain-behavior relationship, we repeated the whole cross-validated CCA procedure, but first age was regressed along with the other covariates before the CCA was performed, referred to as M_2 in the text. This effectively removes the association with age from the subsequent analyses as described in Results. When the RSA analysis is repeated with M_2, the resulting dissimilarity modules reflect the brain-behavior interaction with the variability of age removed. What is left represents the difference between models with and without age. By taking the difference between the S_1 and S_2 we are able to show the impact of age on the brain-behavior relationship (S_d). The difference between these modules is the impact of age on the connection between these scores.

References

Ades-Aron, Benjamin, et al. “Evaluation of the Accuracy and Precision of the Diffusion Parameter EStImation with Gibbs and NoisE Removal Pipeline.” *NeuroImage*, vol. 183, Dec. 2018, pp. 532–43.

Allen, Elena A., et al. “A Baseline for the Multivariate Comparison of Resting-State Networks.” *Frontiers in Systems Neuroscience*, vol. 5, Feb. 2011, p. 2.

Amunts, Julia, et al. “Executive Functions Predict Verbal Fluency Scores in Healthy Participants.” *Scientific Reports*, vol. 10, no. 1, July 2020, p. 11141.

Anderson, Charles. “Docker [Software Engineering].” *IEEE Software*, vol. 32, no. 3, 2015, pp. 102–c3, doi:10.1109/ms.2015.62.

Andlin-Sobocki, Patrik, et al. “Cost of Disorders of the Brain in Europe.” *European Journal of Neurology: The Official Journal of the European Federation of Neurological Societies*, vol. 12, no. s1, Wiley Online Library, 2005, pp. 1–27.

Apostolova, Liana G., et al. “Hippocampal Atrophy and Ventricular Enlargement in Normal Aging, Mild Cognitive Impairment (MCI), and Alzheimer Disease.” *Alzheimer Disease and Associated Disorders*, vol. 26, no. 1, Jan. 2012, pp. 17–27.

Assem, Moataz, et al. “Activity in the Fronto-Parietal Multiple-Demand Network Is Robustly Associated with Individual Differences in Working Memory and Fluid Intelligence.” *Cortex; a Journal Devoted to the Study of the Nervous System and Behavior*, vol. 131, July 2020, pp. 1–16.

Avesani, Paolo, et al. “The Open Diffusion Data Derivatives, Brain Data Upcycling via Integrated Publishing of Derivatives and Reproducible Open Cloud Services.” *Nature Scientific Data*, vol. 6, no. 1, 2019, pp. 1–13.

Bae, Eunseong, et al. “Multi-Group Analysis Using Generalized Additive Kernel Canonical Correlation Analysis.” *Scientific Reports*, vol. 10, no. 1, July 2020, p. 12624.

Bajaj, Sahil, et al. “Brain Aging: Uncovering Cortical Characteristics of Healthy Aging in Young Adults.” *Frontiers in Aging Neuroscience*, vol. 9, Dec. 2017, p. 412.

Bassett, Danielle S., and Olaf Sporns. “Network Neuroscience.” *Nature Neuroscience*, vol. 20, no. 3, Feb. 2017, pp. 353–64.

Beaton, Derek, et al. *Multivariate Genotypic Analyses That Identify Specific Genotypes to Characterize Disease and Control Groups in ADNI*. doi:10.1101/235945.

Beckmann, C. F., and S. M. Smith. “Probabilistic Independent Component Analysis for Functional Magnetic Resonance Imaging.” *IEEE Transactions on Medical Imaging*, vol. 23, no. 2, 2004, pp. 137–52, doi:10.1109/tmi.2003.822821.

Bennett, Patrick J., et al. “The Effects of Aging on Motion Detection and Direction Identification.” *Vision Research*, vol. 47, no. 6, 2007, pp. 799–809, doi:10.1016/j.visres.2007.01.001.

Bijsterbosch, Janine Diane, et al. “The Relationship between Spatial Configuration and Functional Connectivity of Brain Regions Revisited.” *eLife*, vol. 8, May 2019, doi:10.7554/eLife.44890.

Bishop, Nicholas A., et al. “Neural Mechanisms of Ageing and Cognitive Decline.” *Nature*, vol. 464, no. 7288, 2010, pp. 529–35, doi:10.1038/nature08983.

Braun, Urs, et al. “Dynamic Reconfiguration of Frontal Brain Networks during Executive Cognition in Humans.” *Proceedings of the National Academy of Sciences of the United States of America*, vol. 112, no. 37, Sept. 2015, pp. 11678–83.

Buckner, Randy L., et al. “Functional Brain Imaging of Young, Nondemented, and Demented Older Adults.” *Journal of Cognitive Neuroscience*, vol. 12, no. supplement 2, 2000, pp. 24–34, doi:10.1162/089892900564046.

Cabeza, Roberto, et al. *Cognitive Neuroscience of Aging: Linking Cognitive and Cerebral Aging*. Oxford University Press, 2009.

Calhoun, V. D., et al. “A Method for Making Group Inferences from Functional MRI Data Using Independent Component Analysis.” *Human Brain Mapping*, vol. 14, no. 3, Nov. 2001, pp. 140–51.

Calhoun, Vince D., et al. “A Review of Group ICA for fMRI Data and ICA for Joint Inference of Imaging, Genetic, and ERP Data.” *NeuroImage*, vol. 45, no. 1 Suppl, Mar. 2009, pp. S163–72.

Carstensen, Laura L., et al. “Emotional Experience Improves with Age: Evidence Based on over 10 Years of Experience Sampling.” *Psychology and Aging*, vol. 26, no. 1, Mar. 2011, pp. 21–33.

Cepeda, N. J., et al. “Changes in Executive Control across the Life Span: Examination of Task-Switching Performance.” *Developmental Psychology*, vol. 37, no. 5, Sept. 2001, pp. 715–30.

Cheng, Hu, et al. “Optimization of Seed Density in DTI Tractography for Structural Networks.” *Journal of Neuroscience Methods*, vol. 203, no. 1, Jan. 2012, pp. 264–72.

Cole, James, et al. *Quantification of the Biological Age of the Brain Using Neuroimaging*. doi:10.31219/osf.io/3b6zu.

Cole, James H., and Katja Franke. “Predicting Age Using Neuroimaging: Innovative Brain Ageing Biomarkers.” *Trends in Neurosciences*, vol. 40, no. 12, Dec. 2017, pp. 681–90.

Cox, Simon R., et al. “Ageing and Brain White Matter Structure in 3,513 UK Biobank Participants.” *Nature Communications*, vol. 7, no. 1, 2016, doi:10.1038/ncomms13629.

Craik, Fergus I. M., and Ellen Bialystok. “Cognition through the Lifespan: Mechanisms of Change.” *Trends in Cognitive Sciences*, vol. 10, no. 3, 2006, pp. 131–38, doi:10.1016/j.tics.2006.01.007.

Dahne, Sven, et al. “Multivariate Machine Learning Methods for Fusing Multimodal Functional Neuroimaging Data.” *Proceedings of the IEEE*, vol. 103, no. 9, 2015, pp. 1507–30, doi:10.1109/jproc.2015.2425807.

Daianu, Madelaine, et al. “Breakdown of Brain Connectivity between Normal Aging and Alzheimer’s Disease: A Structural K-Core Network Analysis.” *Brain Connectivity*, vol. 3, no. 4, 2013, pp. 407–22.

Davis, Simon W., et al. “Cooperative Contributions of Structural and Functional Connectivity to Successful Memory in Aging.” *Network Neuroscience (Cambridge, Mass.)*, vol. 3, no. 1, 2019, pp. 173–94.

Deary, Ian J., et al. “Age-Associated Cognitive Decline.” *British Medical Bulletin*, vol. 92, no. 1, Oxford Academic, Dec. 2009, pp. 135–52.

D’Esposito, M., et al. “The Effect of Normal Aging on the Coupling of Neural Activity to the Bold Hemodynamic Response.” *NeuroImage*, vol. 10, no. 1, July 1999, pp. 6–14.

Diedrichsen, Jörn, and Nikolaus Kriegeskorte. “Representational Models: A Common Framework for Understanding Encoding, Pattern-Component, and Representational-Similarity Analysis.” *PLoS Computational Biology*, vol. 13, no. 4, Apr. 2017, p. e1005508.

DiLuca, Monica, and Jes Olesen. “The Cost of Brain Diseases: A Burden or a Challenge?” *Neuron*, vol. 82, no. 6, Elsevier, 2014, pp. 1205–08.

Driscoll, Ira, et al. “The Aging Hippocampus: Cognitive, Biochemical and Structural Findings.” *Cerebral Cortex* , vol. 13, no. 12, Dec. 2003, pp. 1344–51.

Du, Lei, et al. “Identifying Diagnosis-Specific Genotype–phenotype Associations via Joint Multitask Sparse Canonical Correlation Analysis and Classification.” *Bioinformatics*, vol. 36, no. Supplement_1, 2020, pp. i371–79, doi:10.1093/bioinformatics/btaa434.

Falk, Emily B., et al. “What Is a Representative Brain? Neuroscience Meets Population Science.” *Proceedings of the National Academy of Sciences of the United States of America*, vol. 110, no. 44, Oct. 2013, pp. 17615–22.

Fischl, Bruce. “FreeSurfer.” *NeuroImage*, vol. 62, no. 2, 2012, pp. 774–81, doi:10.1016/j.neuroimage.2012.01.021.

Fjell, Anders M., et al. “One-Year Brain Atrophy Evident in Healthy Aging.” *The Journal of Neuroscience: The Official Journal of the Society for Neuroscience*, vol. 29, no. 48, Dec. 2009, pp. 15223–31.

Folstein, Marshal F., et al. “Mini-Mental State Examination.” *PsycTESTS Dataset*, 2014, doi:10.1037/t07757-000.

---. “The Mini-Mental State Examination.” *Archives of General Psychiatry*, vol. 40, no. 7, 1983, p. 812, doi:10.1001/archpsyc.1983.01790060110016.

Gaetz, William, et al. “Functional and Structural Correlates of the Aging Brain: Relating Visual Cortex (V1) Gamma Band Responses to Age-related Structural Change.” *Human Brain Mapping*, vol. 33, no. 9, 2012, pp. 2035–46, doi:10.1002/hbm.21339.

Gazzaley, Adam, et al. “Top-down Suppression Deficit Underlies Working Memory Impairment in Normal Aging.” *Nature Neuroscience*, vol. 8, no. 10, Oct. 2005, pp. 1298–300.

Glasser, Matthew F., et al. “A Multi-Modal Parcellation of Human Cerebral Cortex.” *Nature*, vol. 536, no. 7615, Aug. 2016, pp. 171–78.

Gordon, Brian A., et al. “Task-Evoked fMRI Changes in Attention Networks Are Associated with Preclinical Alzheimer’s Disease Biomarkers.” *Neurobiology of Aging*, vol. 36, no. 5, 2015, pp. 1771–79,

doi:10.1016/j.neurobiolaging.2015.01.019.

Grady, Cheryl. “The Cognitive Neuroscience of Ageing.” *Nature Reviews Neuroscience*, vol. 13, no. 7, 2012, pp. 491–505, doi:10.1038/nrn3256.

Grady, Cheryl L., et al. “A Multivariate Analysis of Age-Related Differences in Default Mode and Task-Positive Networks across Multiple Cognitive Domains.” *Cerebral Cortex* , vol. 20, no. 6, June 2010, pp. 1432–47.

Greve, Douglas N., and Bruce Fischl. “Accurate and Robust Brain Image Alignment Using Boundary-Based Registration.” *NeuroImage*, vol. 48, no. 1, Oct. 2009, pp. 63–72.

Guntupalli, J. Swaroop, et al. “A Model of Representational Spaces in Human Cortex.” *Cerebral Cortex* , vol. 26, no. 6, June 2016, pp. 2919–34.

Gustavsson, Anders, et al. “Cost of Disorders of the Brain in Europe 2010.” *European Neuropsychopharmacology: The Journal of the European College of Neuropsychopharmacology*, vol. 21, no. 10, Oct. 2011, pp. 718–79.

Gutchess, Angela. “Plasticity of the Aging Brain: New Directions in Cognitive Neuroscience.” *Science*, vol. 346, no. 6209, Oct. 2014, pp. 579–82.

Habes, M., et al. “Advanced Brain Aging: Relationship with Epidemiologic and Genetic Risk Factors, and Overlap with Alzheimer Disease Atrophy Patterns.” *Translational Psychiatry*, vol. 6, Apr. 2016, p. e775.

Hao, Xiaoke, et al. “Identification of Associations between Genotypes and Longitudinal Phenotypes via Temporally-Constrained Group Sparse Canonical Correlation Analysis.” *Bioinformatics* , vol. 33, no. 14, July 2017, pp. i341–49.

Harada, Caroline N., et al. “Normal Cognitive Aging.” *Clinics in Geriatric Medicine*, vol. 29, no. 4, 2013, pp. 737–52, doi:10.1016/j.cger.2013.07.002.

Hawrylycz, Michael J., et al. “An Anatomically Comprehensive Atlas of the Adult Human Brain Transcriptome.” *Nature*, vol. 489, no. 7416, Sept. 2012, pp. 391–99.

Helmer, Markus, et al. *On Stability of Canonical Correlation Analysis and Partial Least Squares with Application to Brain-Behavior Associations*. 25 Aug. 2020, p. 2020.08.25.265546, doi:10.1101/2020.08.25.265546.

Hsu, Lauren L., and Aedin C. Culhane. “Impact of Data Preprocessing on Integrative Matrix Factorization of Single Cell Data.” *Frontiers in Oncology*, vol. 10, June 2020, p. 973.

Huettel, S. A., et al. “The Effects of Aging upon the Hemodynamic Response Measured by Functional MRI.” *NeuroImage*, vol. 13, no. 1, Jan. 2001, pp. 161–75.

Huk, Alexander C. “Multiplexing in the Primate Motion Pathway.” *Vision Research*, vol. 62, 2012, pp. 173–80, doi:10.1016/j.visres.2012.04.007.

Jeurissen, Ben, et al. “Multi-Tissue Constrained Spherical Deconvolution for Improved Analysis of Multi-Shell Diffusion MRI

Data." *NeuroImage*, vol. 103, 2014, pp. 411–26, doi:10.1016/j.neuroimage.2014.07.061.

Johnson, S. C., et al. "The Relationship between fMRI Activation and Cerebral Atrophy: Comparison of Normal Aging and Alzheimer Disease." *NeuroImage*, vol. 11, no. 3, Mar. 2000, pp. 179–87.

Khambhati, Ankit N., et al. "Beyond Modularity: Fine-Scale Mechanisms and Rules for Brain Network Reconfiguration." *NeuroImage*, vol. 166, Feb. 2018, pp. 385–99.

Kong, Tania S., et al. "Age-Related Differences in Functional Brain Network Segregation Are Consistent with a Cascade of Cerebrovascular, Structural, and Cognitive Effects." *Network Neuroscience (Cambridge, Mass.)*, vol. 4, no. 1, Feb. 2020, pp. 89–114.

Kramer, Arthur F., et al. "Task Coordination and Aging: Explorations of Executive Control Processes in the Task Switching Paradigm." *Acta Psychologica*, vol. 101, no. 2-3, 1999, pp. 339–78, doi:10.1016/s0001-6918(99)00011-6.

Kriegeskorte, Nikolaus. "Representational Similarity Analysis – Connecting the Branches of Systems Neuroscience." *Frontiers in Systems Neuroscience*, 2008, doi:10.3389/neuro.06.004.2008.

Krishnan, Anjali, et al. "Partial Least Squares (PLS) Methods for Neuroimaging: A Tutorial and Review." *NeuroImage*, vol. 56, no. 2, May 2011, pp. 455–75.

Kurtzer, Gregory M., et al. "Singularity: Scientific Containers for Mobility of Compute." *PloS One*, vol. 12, no. 5, May 2017, p. e0177459.

Li, Hui-Jie, et al. "Putting Age-Related Task Activation into Large-Scale Brain Networks: A Meta-Analysis of 114 fMRI Studies on Healthy Aging." *Neuroscience and Biobehavioral Reviews*, vol. 57, Oct. 2015, pp. 156–74.

Li, Qiongge, et al. "Longitudinal Changes in Whole-Brain Functional Connectivity Strength Patterns and the Relationship With the Global Cognitive Decline in Older Adults." *Frontiers in Aging Neuroscience*, vol. 12, 2020, doi:10.3389/fnagi.2020.00071.

Lisman, John, et al. "Publisher Correction: Viewpoints: How the Hippocampus Contributes to Memory, Navigation and Cognition." *Nature Neuroscience*, vol. 21, no. 7, 2018, pp. 1018–1018, doi:10.1038/s41593-017-0034-8.

Llera, Alberto, et al. "Inter-Individual Differences in Human Brain Structure and Morphology Link to Variation in Demographics and Behavior." *eLife*, vol. 8, July 2019, doi:10.7554/eLife.44443.

Lustig, Cindy, et al. "Aging, Training, and the Brain: A Review and Future Directions." *Neuropsychology Review*, vol. 19, no. 4, 2009, pp. 504–22, doi:10.1007/s11065-009-9119-9.

Lu, Zhong-Lin, et al. "Fast Decay of Iconic Memory in Observers with Mild Cognitive Impairments." *Proceedings of the National Academy of Sciences of the United States of America*, vol. 102, no. 5, Feb. 2005, pp. 1797–802.

Lydon-Staley, David M., et al. "Modeling Brain, Symptom, and Behavior in the Winds of Change." *Neuropsychopharmacology: Official Publication of the American College of Neuropsychopharmacology*, Aug. 2020, doi:10.1038/s41386-020-00805-6.

Maillet, David, and M. Natasha Rajah. “Association between Prefrontal Activity and Volume Change in Prefrontal and Medial Temporal Lobes in Aging and Dementia: A Review.” *Ageing Research Reviews*, vol. 12, no. 2, Mar. 2013, pp. 479–89.

Marek, Scott, et al. *Towards Reproducible Brain-Wide Association Studies*. 22 Aug. 2020, p. 2020.08.21.257758, doi:10.1101/2020.08.21.257758.

Maunsell, John H. R. “Neuronal Representations of Cognitive State: Reward or Attention?” *Trends in Cognitive Sciences*, vol. 8, no. 6, June 2004, pp. 261–65.

McIntosh, Anthony Randal, and Nancy J. Lobaugh. “Partial Least Squares Analysis of Neuroimaging Data: Applications and Advances.” *NeuroImage*, vol. 23 Suppl 1, 2004, pp. S250–63.

McIntosh, Anthony R., and Bratislav Mišić. “Multivariate Statistical Analyses for Neuroimaging Data.” *Annual Review of Psychology*, vol. 64, 2013, pp. 499–525.

Milham, Michael P., et al. “Attentional Control in the Aging Brain: Insights from an fMRI Study of the Stroop Task.” *Brain and Cognition*, vol. 49, no. 3, 2002, pp. 277–96, doi:10.1006/brcg.2001.1501.

Mok, Robert M., et al. “Behavioral and Neural Markers of Flexible Attention over Working Memory in Aging.” *Cerebral Cortex*, vol. 26, no. 4, 2016, pp. 1831–42, doi:10.1093/cercor/bhw011.

Morgan, Sarah E., et al. “A Network Neuroscience Approach to Typical and Atypical Brain Development.” *Biological Psychiatry. Cognitive Neuroscience and Neuroimaging*, vol. 3, no. 9, Sept. 2018, pp. 754–66.

Mueller, Ralph O., and Gregory R. Hancock. “Structural Equation Modeling.” *The Reviewer’s Guide to Quantitative Methods in the Social Sciences*, 2018, pp. 445–56, doi:10.4324/9781315755649-33.

Mueller, Susanne G., et al. “Ways toward an Early Diagnosis in Alzheimer’s Disease: The Alzheimer's Disease Neuroimaging Initiative (ADNI).” *Alzheimer’s & Dementia*, vol. 1, no. 1, 2005, pp. 55–66, doi:10.1016/j.jalz.2005.06.003.

Nations, United, and United Nations. *World Population Ageing 2019 Highlights*. 2019, doi:10.18356/9df3caed-en.

Niccoli, Teresa, and Linda Partridge. “Ageing as a Risk Factor for Disease.” *Current Biology*, vol. 22, no. 17, 2012, pp. R741–52, doi:10.1016/j.cub.2012.07.024.

Nyberg, Lars, and Sara Pudas. “Successful Memory Aging.” *Annual Review of Psychology*, vol. 70, Jan. 2019, pp. 219–43.

Oschwald, Jessica, et al. “Brain Structure and Cognitive Ability in Healthy Aging: A Review on Longitudinal Correlated Change.” *Reviews in the Neurosciences*, vol. 31, no. 1, Dec. 2019, pp. 1–57.

Park, Denise C., and Patricia Reuter-Lorenz. “The Adaptive Brain: Aging and Neurocognitive Scaffolding.” *Annual Review of Psychology*, vol. 60, 2009, pp. 173–96.

Patenaude, Brian, et al. “A Bayesian Model of Shape and Appearance for Subcortical Brain Segmentation.” *NeuroImage*, vol. 56, no. 3, 2011, pp. 907–22, doi:10.1016/j.neuroimage.2011.02.046.

Paxton, Jessica L., et al. “Cognitive Control, Goal Maintenance, and Prefrontal Function in Healthy Aging.” *Cerebral Cortex* ,

vol. 18, no. 5, May 2008, pp. 1010–28.

Petersen, Steven E., and Olaf Sporns. “Brain Networks and Cognitive Architectures.” *Neuron*, vol. 88, no. 1, 2015, pp. 207–19, doi:10.1016/j.neuron.2015.09.027.

Poldrack, Russell A. “Mapping Mental Function to Brain Structure: How Can Cognitive Neuroimaging Succeed?” *Perspectives on Psychological Science: A Journal of the Association for Psychological Science*, vol. 5, no. 6, Nov. 2010, pp. 753–61.

Ratcliff, Roger, Anjali Thapar, Pablo Gomez, et al. “A Diffusion Model Analysis of the Effects of Aging in the Lexical-Decision Task.” *Psychology and Aging*, vol. 19, no. 2, June 2004, pp. 278–89.

Ratcliff, Roger, Anjali Thapar, and Gail McKoon. “A Diffusion Model Analysis of the Effects of Aging on Brightness Discrimination.” *Perception & Psychophysics*, vol. 65, no. 4, May 2003, pp. 523–35.

Reisberg, Barry, et al. “Evidence and Mechanisms of Retrogenesis in Alzheimer’s and Other Dementias: Management and Treatment Import.” *American Journal of Alzheimer’s Disease & Other Dementiasr*, vol. 17, no. 4, 2002, pp. 202–12, doi:10.1177/153331750201700411.

Reuter-Lorenz, Patricia A., and Cindy Lustig. “Brain Aging: Reorganizing Discoveries about the Aging Mind.” *Current Opinion in Neurobiology*, vol. 15, no. 2, Apr. 2005, pp. 245–51.

Rex, David E., et al. “The LONI Pipeline Processing Environment.” *NeuroImage*, vol. 19, no. 3, July 2003, pp. 1033–48.

Rich, Preston B., and Noran Barry. “Health-Care Economics and the Impact of Aging on Rising Health-Care Costs.” *Geriatric Trauma and Critical Care*, 2017, pp. 99–105, doi:10.1007/978-3-319-48687-1_11.

Risacher, Shannon L., and Andrew J. Saykin. “Neuroimaging in Aging and Neurologic Diseases.” *Handbook of Clinical Neurology*, 2019, pp. 191–227, doi:10.1016/b978-0-12-804766-8.00012-1.

Roberts, James A., et al. “Consistency-Based Thresholding of the Human Connectome.” *NeuroImage*, vol. 145, 2017, pp. 118–29, doi:10.1016/j.neuroimage.2016.09.053.

Rubinov, Mikail, and Olaf Sporns. “Complex Network Measures of Brain Connectivity: Uses and Interpretations.” *NeuroImage*, vol. 52, no. 3, Sept. 2010, pp. 1059–69.

Rutter, Lauren A., et al. “Heterogeneous Indicators of Cognitive Performance and Performance Variability Across the Lifespan.” *Frontiers in Aging Neuroscience*, vol. 12, Mar. 2020, p. 62.

Salat, David H., et al. “Thinning of the Cerebral Cortex in Aging.” *Cerebral Cortex* , vol. 14, no. 7, July 2004, pp. 721–30.

Salthouse, Timothy A. “Neuroanatomical Substrates of Age-Related Cognitive Decline.” *Psychological Bulletin*, vol. 137, no. 5, Sept. 2011, pp. 753–84.

---. *Theoretical Perspectives on Cognitive Aging*. 2016, doi:10.4324/9781315785363.

---. “Trajectories of Normal Cognitive Aging.” *Psychology and Aging*, vol. 34, no. 1, 2019, pp. 17–24, doi:10.1037/pag0000288.

---. “What and When of Cognitive Aging.” *Current Directions in Psychological Science*, vol. 13, no. 4, 2004, pp. 140–44,

doi:10.1111/j.0963-7214.2004.00293.x.

Samanez-Larkin, Gregory R., et al. “Selective Attention to Emotion in the Aging Brain.” *Psychology and Aging*, vol. 24, no. 3, Sept. 2009, pp. 519–29.

Schulz, Marc-Andre, et al. “Different Scaling of Linear Models and Deep Learning in UKBiobank Brain Images versus Machine-Learning Datasets.” *Nature Communications*, vol. 11, no. 1, 2020, doi:10.1038/s41467-020-18037-z.

Sekuler, R., and L. P. Hutman. “Spatial Vision and Aging. I: Contrast Sensitivity.” *Journal of Gerontology*, vol. 35, no. 5, 1980, pp. 692–99, doi:10.1093/geronj/35.5.692.

Semedo, João D., et al. “Cortical Areas Interact through a Communication Subspace.” *Neuron*, vol. 102, no. 1, Apr. 2019, pp. 249–59.e4.

Shafto, Meredith A., et al. “The Cambridge Centre for Ageing and Neuroscience (Cam-CAN) Study Protocol: A Cross-Sectional, Lifespan, Multidisciplinary Examination of Healthy Cognitive Ageing.” *BMC Neurology*, vol. 14, Oct. 2014, p. 204.

Shirer, W. R., et al. “Decoding Subject-Driven Cognitive States with Whole-Brain Connectivity Patterns.” *Cerebral Cortex* , vol. 22, no. 1, Jan. 2012, pp. 158–65.

Silva, Rogers F., et al. “A Statistically Motivated Framework for Simulation of Stochastic Data Fusion Models Applied to Multimodal Neuroimaging.” *NeuroImage*, vol. 102 Pt 1, Nov. 2014, pp. 92–117.

Singanamalli, Asha, et al. “Cascaded Multi-View Canonical Correlation (CaMCCo) for Early Diagnosis of Alzheimer’s Disease via Fusion of Clinical, Imaging and Omic Features.” *Scientific Reports*, vol. 7, no. 1, 2017, doi:10.1038/s41598-017-03925-0.

Smith, Robert E., et al. “Anatomically-Constrained Tractography: Improved Diffusion MRI Streamlines Tractography through Effective Use of Anatomical Information.” *NeuroImage*, vol. 62, no. 3, 2012, pp. 1924–38, doi:10.1016/j.neuroimage.2012.06.005.

Smith, Stephen M., et al. “A Positive-Negative Mode of Population Covariation Links Brain Connectivity, Demographics and Behavior.” *Nature Neuroscience*, vol. 18, no. 11, Nov. 2015, pp. 1565–67.

Svaldi, Diana Otero, et al. “IC-P-032: IMPROVING PREDICTION OF COGNITIVE OUTCOMES FROM FUNCTIONAL CONNECTIVITY IN ALZHEIMER’S DISEASE.” *Alzheimer’s & Dementia*, vol. 15, 2019, pp. P38–39, doi:10.1016/j.jalz.2019.06.4194.

Takemura, Hiromasa, et al. “Ensemble Tractography.” *PLoS Computational Biology*, vol. 12, no. 2, Feb. 2016, p. e1004692.

Taylor, Warren D., et al. “Can We Change the Inevitable? Ameliorating Brain Aging and Cognitive Decline.” *The American Journal of Geriatric Psychiatry*, vol. 24, no. 3, 2016, p. S7, doi:10.1016/j.jagp.2016.01.008.

Thapar, Anjali, et al. “A Diffusion Model Analysis of the Effects of Aging on Letter Discrimination.” *Psychology and Aging*, vol.

18, no. 3, Sept. 2003, pp. 415–29.

Thomason, Moriah E., and Paul M. Thompson. “Diffusion Imaging, White Matter, and Psychopathology.” *Annual Review of Clinical Psychology*, vol. 7, no. 1, 2011, pp. 63–85, doi:10.1146/annurev-clinpsy-032210-104507.

Thompson, Paul M., et al. “ENIGMA and the Individual: Predicting Factors That Affect the Brain in 35 Countries Worldwide.” *NeuroImage*, vol. 145, no. Pt B, Jan. 2017, pp. 389–408.

Tournier, J. Donald, et al. “MRtrix3: A Fast, Flexible and Open Software Framework for Medical Image Processing and Visualisation.” *NeuroImage*, vol. 202, Nov. 2019, p. 116137.

Tsvetanov, Kamen A., et al. “Extrinsic and Intrinsic Brain Network Connectivity Maintains Cognition across the Lifespan Despite Accelerated Decay of Regional Brain Activation.” *The Journal of Neuroscience: The Official Journal of the Society for Neuroscience*, vol. 36, no. 11, Mar. 2016, pp. 3115–26.

Turner, Brandon M., et al. “Approaches to Analysis in Model-Based Cognitive Neuroscience.” *Journal of Mathematical Psychology*, vol. 76, no. B, Feb. 2017, pp. 65–79.

van den Heuvel, Martijn P., and Olaf Sporns. “A Cross-Disorder Connectome Landscape of Brain Dysconnectivity.” *Nature Reviews. Neuroscience*, vol. 20, no. 7, July 2019, pp. 435–46.

Van Essen, D. C., and K. Ugurbil. “The Future of the Human Connectome.” *NeuroImage*, vol. 62, no. 2, 2012, pp. 1299–310, doi:10.1016/j.neuroimage.2012.01.032.

Veitch, Dallas P., et al. “Understanding Disease Progression and Improving Alzheimer’s Disease Clinical Trials: Recent Highlights from the Alzheimer's Disease Neuroimaging Initiative.” *Alzheimer’s & Dementia*, vol. 15, no. 1, 2019, pp. 106–52, doi:10.1016/j.jalz.2018.08.005.

Vinke, Elisabeth J., et al. “Trajectories of Imaging Markers in Brain Aging: The Rotterdam Study.” *Neurobiology of Aging*, vol. 71, Nov. 2018, pp. 32–40.

Wandell, Brian A. “Clarifying Human White Matter.” *Annual Review of Neuroscience*, vol. 39, July 2016, pp. 103–28.

Wang, Hao-Ting, et al. “Finding the Needle in a High-Dimensional Haystack: Canonical Correlation Analysis for Neuroscientists.” *NeuroImage*, vol. 216, 2020, p. 116745, doi:10.1016/j.neuroimage.2020.116745.

Weiner, Michael W., et al. “Recent Publications from the Alzheimer’s Disease Neuroimaging Initiative: Reviewing Progress toward Improved AD Clinical Trials.” *Alzheimer’s & Dementia*, vol. 13, no. 4, 2017, pp. e1–85, doi:10.1016/j.jalz.2016.11.007.

Westlye, L. T., et al. “Life-Span Changes of the Human Brain White Matter: Diffusion Tensor Imaging (DTI) and Volumetry.” *Cerebral Cortex*, vol. 20, no. 9, 2010, pp. 2055–68, doi:10.1093/cercor/bhp280.

Wittchen, H. U., et al. “The Size and Burden of Mental Disorders and Other Disorders of the Brain in Europe 2010.” *European Neuropsychopharmacology: The Journal of the European College of Neuropsychopharmacology*, vol. 21, no. 9, Sept.

2011, pp. 655–79.

Wykes, Til, et al. “Mental Health Research Priorities for Europe.” *The Lancet. Psychiatry*, vol. 2, no. 11, Nov. 2015, pp. 1036–42.

Xu, Ting, et al. “A Connectome Computation System for Discovery Science of Brain.” *Science Bulletin*, vol. 60, no. 1, 2015, pp. 86–95, doi:10.1007/s11434-014-0698-3.

Yeatman, Jason D., et al. “Lifespan Maturation and Degeneration of Human Brain White Matter.” *Nature Communications*, vol. 5, no. 1, 2014, doi:10.1038/ncomms5932.

Yeo, B. T. Thomas, et al. “The Organization of the Human Cerebral Cortex Estimated by Intrinsic Functional Connectivity.” *Journal of Neurophysiology*, vol. 106, no. 3, Sept. 2011, pp. 1125–65.

Zuo, Xi-Nian, et al. “Human Connectomics across the Life Span.” *Trends in Cognitive Sciences*, vol. 21, no. 1, Jan. 2017, pp. 32–45.